

Rings beyond the giant planets

BRUNO SICARDY, MARYAME EL MOUTAMID, ALICE C. QUILLEN,
PAUL M. SCHENK, MARK R. SHOWALTER, AND KEVIN WALSH

arXiv:1612.03321v2 [astro-ph.EP] 11 Apr 2017

7.1 Introduction

Until 2013, only the giant planets were known to host ring systems. In June 2013, a stellar occultation revealed the presence of narrow and dense rings around Chariklo, a small Centaur object that orbits between Saturn and Uranus. Meanwhile, the Cassini spacecraft revealed evidence for the possible past presence of rings around the Saturnian satellites Rhea and Iapetus. Mars and Pluto are expected to have tenuous dusty rings, though they have so far evaded detection. More remotely, transit events observed around a star in 2007 may have revealed for the first time exoplanetary rings around a giant planet orbiting that star.

So, evidence is building to show that rings are more common features in the universe than previously thought. Several interesting issues arise from the discovery (or suspicion) of the new ring systems described in this chapter. One of them is to assess how universal is the physics governing rings, in spite of large differences in size, age and origin. In other words, do rings obey some common, fundamental processes, or are their similarities just apparent and stemming from very different mechanisms? Another interesting question is what those ring systems tell us about the origin, evolution and physical properties of the bodies they encircle. As such, rings may be of precious help to better understand the formation of satellites and planets, not only in our own solar system, but also among extrasolar worlds. We will return to those considerations in the concluding remarks of this chapter, after reviewing recent ring system discoveries.

7.2 Dense rings around the small Centaur object Chariklo

In June 2013, narrow, sharply confined dense rings were discovered around the small Centaur object (10199) Chariklo. This asteroid-like object became the first body of the solar system, other than the giant planets, known to possess rings. Meanwhile, those rings resemble some of the sharply defined features observed around Saturn or Uranus (Figs. 7.1-7.3), suggesting some common dynamics.

Centaur objects are small objects (diameters less than about 250 km) with perihelion beyond Jupiter’s orbit (5.2 AU) and semi-major axis inside of Neptune (30.0 AU). They were originally Trans-Neptunian Objects (TNO’s) that have been

scattered by gravitational tugs from Neptune or Uranus (Gladman et al., 2008).

Chariklo was discovered in February 1997 (Scotti, 1997) and is the largest Centaur known to date, with a diameter of about 240 km. Its very low geometric albedo (about 4%, see Table 7.1) makes it one of the darkest objects of the solar system. It moves close to a 4:3 mean-motion resonance with Uranus, its main perturber. Dynamical studies indicate that Chariklo has been captured in its present orbital configuration some 10 Myr ago, and that the half-life time of its unstable current orbit is about 10 Myr (Horner et al., 2004), a very short timescale compared to the age of the solar system.

Year-scale photometric (Belskaya et al., 2010) and spectroscopic (Guilbert-Lepoutre, 2011) variations of Chariklo were tentatively attributed to transient periods of cometary activity. As discussed below, those variations can be naturally explained by the presence of a flat, partially icy ring system observed at various aspect angles, so that no cometary activity is necessary to explain this behavior. Actually, we will see that no dust or gas production has been detected so far around Chariklo.

Meanwhile, Chiron (another Centaur similar in size to Chariklo) is also surrounded by narrowly confined material whose interpretation is still debated. This shows that material around Centaurs or other small bodies may be more common than previously thought.

In the following sub-sections, the term “Chariklo” will apply to the central body only, while “Chariklo’s system” will denote the entire set Chariklo plus its rings.

7.2.1 The discovery of Chariklo’s rings

Chariklo’s rings were discovered during a stellar occultation, which occurs when an object passes in front of a star, blocking its flux for some seconds (Fig. 7.2). Such an event was monitored on June 3, 2013 from various sites in Brazil, Uruguay, Argentina and Chile, see Fig. 7.1 and Braga-Ribas et al. (2014). This was the first successful Chariklo occultation ever observed. This event was one of a number aimed at characterizing the sizes, shapes and surroundings of TNO’s and Centaurs (Assafin et al., 2012; Camargo et al., 2014), and monitoring Pluto’s atmosphere (Assafin et al., 2010). In the case of Chariklo, a further incentive was the search for surrounding (possibly cometary) material, as both sharp and diffuse secondary events were detected in 1993 and 1994

Table 7.1. *Chariklo main body physical parameters*

Semi-major axis, period ^a	15.79 AU, 62.71 yrs
Eccentricity, inclination ^a	0.1716, 23.37 deg
Perihelion-aphelion ^a	13.08–18.50 AU
Equivalent radius ^{b,c}	$R_{\text{equiv}} = 119 \pm 5$ km
Visible geometric albedo ^b	$p_V = 0.042 \pm 0.005$
Synodical rotation period ^b	$P_C = 7.004 \pm 0.036$ h
Mass ^d	$\sim 10^{19}$ kg
Surface composition ^e	$\sim 60\%$ amorphous carbon $\sim 30\%$ silicates, $\sim 10\%$ organics

^aDesmars (2015); Desmars et al. (2015). ^bFornasier et al. (2014). ^cThe radius of a spherical body that presents the same apparent surface area as the actual body. ^dOrder of magnitude estimate, using R_{equiv} above and assuming an icy body. ^eDuffard et al. (2014a).

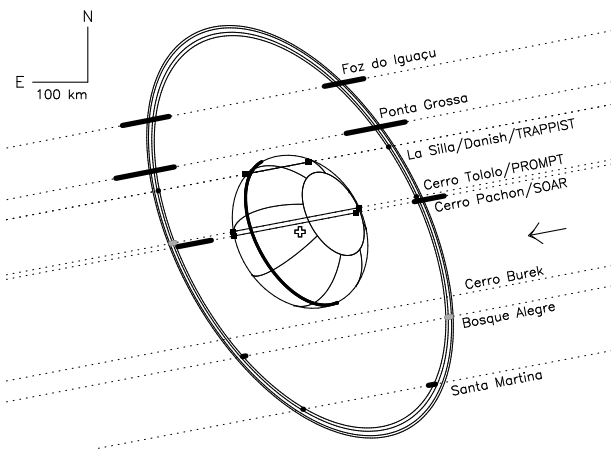


Figure 7.1 The discovery of Chariklo’s rings during the June 3, 2013 stellar occultation. The dotted lines show the trajectories of the star in the plane of the sky relative to Chariklo, as seen from eight stations in Brazil, Argentina and Chile (the arrow indicates the direction of motion). The occultation by the main body was observed along the three black segments - or “chords” - near the center of the plot. Beside these detections, secondary events were observed somewhere inside the black, thick intervals, most of them unresolved in time. Some segments are longer because of the longer integration time used at the corresponding stations, hence their larger uncertainties in position. The two gray segments along the Bosque Alegre and Cerro Tololo chords correspond to dead-times (due to image readouts) during acquisition, leading to *non* detections of the ring, but still providing constraints on the ring location. The rings were not detected at Cerro Burek due to a large integration time at low signal-to-noise ratio. The size, shape and orientation of the inner, denser ring (C1R) is obtained through an elliptical fit to the black and gray segments, weighted with their respective uncertainties. The outer, fainter ring (C2R) was resolved only in the best-sampled light curve of the Danish telescope at La Silla (Fig. 7.2). Its orbit has been reconstructed assuming that C1R and C2R are concentric. Adapted from Braga-Ribas et al. (2014).

during stellar occultations by its sibling Chiron (Elliot et al., 1995; Bus et al., 1996), see below.

Narrow secondary events were indeed detected during the June 2013 event (Figs. 7.1 and 7.2), but it became rapidly

clear that they could not be interpreted as collimated, radial cometary jets ejected from Chariklo’s surface because their geometries were mutually inconsistent with that interpretation. Instead, the ring interpretation was the simplest, although surprising, explanation for all the observed secondary events. All the detections were in fact consistent with the presence of two rings: an inner, denser ring, 2013C1R (C1R for short), orbiting at some 390 km from Chariklo’s center, 15 km inside another, more tenuous outer ring, C2R (Fig. 7.1, Table 7.2). There were several arguments in favor of the ring interpretation drawn from those observations:

- Although most of the stations appearing in Fig. 7.1 did not resolve the rings, their equivalent widths W_e (which measure the amount of material contained in the rings, see Chapter 4) were essentially the same for all events. Such coincidence is hard to reconcile with a set of independent cometary jets going in different directions.
- A flat ring system offers a natural explanation for Chariklo’s long-term photometric variations (see Belskaya et al. 2010 and Fig. 7.4). Those variations merely reflect the changing ring aspect as Chariklo and Earth revolve around the Sun.
- The ring interpretation also offers a simple explanation for the appearance and disappearance of the $2.2 \mu\text{m}$ water ice band in Chariklo’s spectra (Guilbert-Lepoutre 2011 and Fig. 7.5). Again, the changing ring geometry causes the disappearance and reappearance of the ice band, showing by the same token that the rings do contain water ice.

Another occultation observed on April 29, 2014 fully confirmed the ring interpretation drawn from the June 2013 discovery, and revealed finer structures in the main ring C1R, see Fig. 7.3 and the associated discussion. Other occultations revealed either the main body only or the rings alone, but with lower signal-to-noise ratios or insufficient resolution to reveal ring sub-structures (Bérard et al. 2016 and Leiva et al. 2016, in preparation).

7.2.2 Physical properties

7.2.2.1 Orbit

The secondary events shown around Chariklo in Fig. 7.1 constrain the apparent shape, size and orientation of the

Table 7.2. *Chariklo's rings physical parameters*

	Radius ^a	Radial width	Normal optical depth
Ring C1R	390.6 ± 3.3 km	4.8 < W < 7.1 km ^b	average $\tau_N \sim 0.4^c$
Ring C2R	404.8 ± 3.3 km	W ~ 1-3 km	$\tau_N \sim 0.1$
Gap between C1R and C2R ^a		8.7 ± 0.4 km	< 0.004
Pole position ^a	$\alpha_p = 10 \text{ h } 05 \text{ min} \pm 02 \text{ min}$, $\delta_p = +41^\circ 29' \pm 13'$ (equatorial J2000)		
Visible reflectivity ^d	$(I/F)_V = 0.07 \pm 0.01$		
Surface composition ^d	20% water ice, 40-70% silicates, 10-30% tholins, small quantities of amorphous carbon		

^aFrom Braga-Ribas et al. (2014), assuming circular rings. ^bSmallest and largest widths observed during the June 3, 2013 and April 29, 2014 stellar occultations (Sicardy et al., 2014, and Bérard et al. 2016, in preparation). ^cWith some some opaque parts, see text and Fig. 7.3. ^dDuffard et al. (2014a).

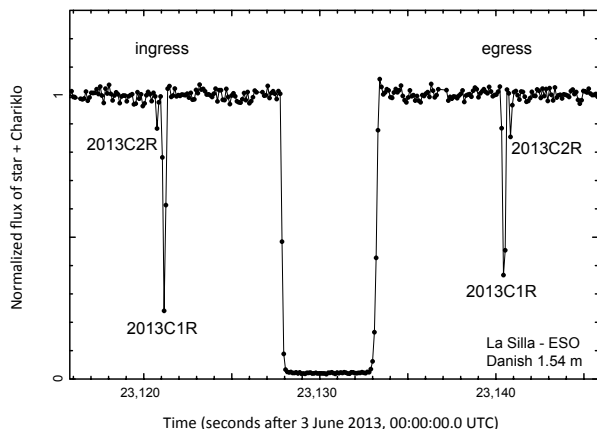


Figure 7.2 Plot of the stellar flux vs. time, as observed from the Danish telescope at La Silla, during the June 3, 2013 occultation. This is the best sampled at highest signal-to-noise ratio light curve among the various sites involved in this observation (Fig. 7.1). It shows a ~ 5.3 s central drop, corresponding to the blocking of the stellar flux by Chariklo’s main body. The two symmetric events on each side are caused by the rings. In fact, each event is resolved into a main (C1R) and fainter (C2R) rings separated by an essentially empty gap. Adapted from Braga-Ribas et al. (2014).

main ring C1R projected in the sky plane (the case of the more tenuous, nearby ring C2R is considered in a second step, as mentioned in the caption of Fig. 7.1).

The simplest model for ring C1R is that of an ellipse with one focus at Chariklo’s center of mass. However, we do not know a priori the ring pole position, nor its apse orientation. Moreover, we do not have enough occulting chords across the main body from the observation of June 2013 (nor from other later ones, to date) to determine Chariklo’s center position relative to the main ring (Fig. 7.1).

Thus, one has to make the simplifying assumption that Ring C1R is circular, with opening angle B and position angle P as seen from Earth. An elliptical fit to the secondary events of Fig. 7.1 then provides the center of the ellipse, its apparent semi-major and semi-minor axes a' and b' (projected in the sky plane) and its position angle. Note that in the circular assumption, $|\sin(B)| = b'/a'$.

The elliptical fit displayed in Fig. 7.1 allows two alternative ring pole positions, depending on which part of the ring is “in front” the sky plane. This ambiguity can be solved by considering Chariklo’s photometric evolution over time. The pole position adopted here (Table 7.2) predicts that the rings were observed edge-on in 2008, in agreement with Chariklo’s system photometric behavior (Fig. 7.4). Conversely, the alternative solution predicts an edge-on configuration in 1994 that is out of phase compared to the observed behavior. Moreover, the solution adopted here was confirmed during another Chariklo stellar occultation observed on April 29, 2014 (Bérard et al. 2016, in preparation). Defining the ring pole direction as being parallel to the ring angular momentum, there is a further ambiguity since two opposite orbital motions are possible, that correspond to opposite values of B . We have arbitrarily chosen $B > 0$ in Table 7.2. This choice may be revised in the future (in favor of the opposite pole) if the particles orbital can be determined.

The best light curve obtained during the June 3, 2013 occultation shows that there are actually two rings. The dense ring C1R is flanked by a more tenuous outer ring, C2R (Fig. 7.2). All the other instruments used during the discovery observation did not have enough time resolution to separate the two rings, but they were clearly resolved again during the April 29, 2014 event (Fig. 7.3). The orbital parameters for C1R and C2R, resulting from the fit of Fig. 7.1, are listed in Table 7.2. It is assumed here that C2R has also a circular orbit, 14.2 km outside C1R and concentric with it, as derived by Braga-Ribas et al. (2014).

7.2.2.2 Fine structure

From the June 3, 2013 discovery observations, no material was detected in the gap between C1R and C2R up to a normal optical depth of about 0.004 (Braga-Ribas et al., 2014). Those observations did not reveal structures inside C1R and C2R, due to insufficient time resolution (Fig. 7.2). However, data obtained at higher rate during another event (April 29, 2014) revealed a double-dip structure inside ring C1R, while no structure has been identified so far in the shallower C2R profiles (Fig. 7.3).

The densest parts of C1R are consistent with opaque material concentrated at very sharp edges. The main smooth-

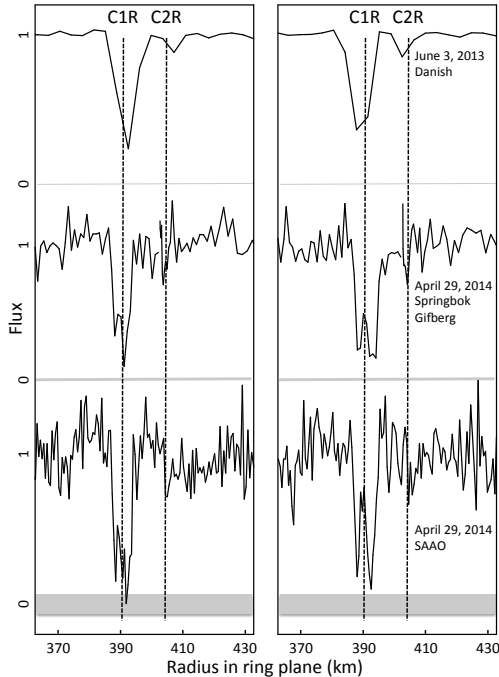


Figure 7.3 Chariklo’s ring radial profiles derived from the June 3, 2013 stellar occultation (Danish telescope, top), the April 29, 2014 combined event at Springbok and Gifberg stations (middle), and the same event at the South African Astronomical Observatory (SAAO, bottom). The gray boxes correspond to the zero stellar fluxes (complete star disappearance), where its thickness represents photometric uncertainties, while unity corresponds to the full, unocculted stellar flux. The horizontal axis is the distance to Chariklo’s center, measured in the plane of the rings, using the orientation given in Table 7.2. This orientation is derived *assuming* that the rings are circular, so that this plot cannot be used to assess or put upper limit on the ring eccentricities. The vertical dotted lines are the ring radii adopted in Table 7.2. Due to the different acquisition rates and viewing geometries, the light curves have radial samplings of 3.6, 1.0 and 0.57 km per data point in the top, middle and bottom panels, respectively. The best resolved profiles are eventually diffraction-limited at the Fresnel scale limit (about 0.8 km). They show sharp edges and a W-shaped structure in the main ring C1R, as well as a width variation for ring C1R.

ing effect of the April 29, 2014 profiles is Fresnel diffraction, which amounts to about 0.8 km when projected at the ring (the finite stellar diameter being negligible for that event). At this scale, one cannot resolve the edges, as the occultation profiles are compatible with infinitely sharp boundaries (Bérard et al. 2016, in preparation).

So far, only eight C1R profiles obtained in 2013 and 2014 could provide an estimation the ring radial width W (projected in the ring plane), the other profiles having insufficient resolution to do so. The width W shows significant variations between 4.8 and 7.1 km (Sicardy et al. 2014 and Table 7.2), with dynamical implications that are discussed later.

For the unresolved profiles, it is possible to estimate the equivalent width $W_{e(1+2)} = (W_1 \cdot p_{N1} + W_2 \cdot p_{N2})$ of the

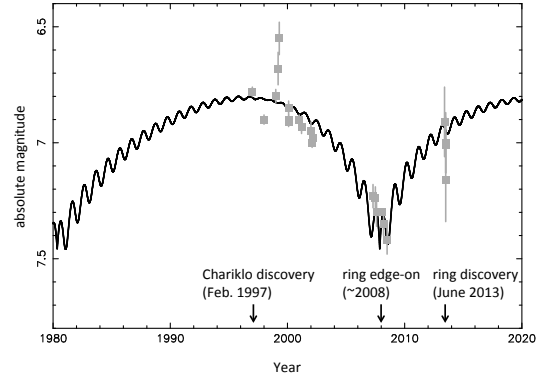


Figure 7.4 The observed absolute magnitude of Chariklo’s system (gray squares) are fitted by a model (black line) that accounts for both the ring and Chariklo contributions to the total observed flux (see Eq. 7.2). Adapted from Duffard et al. (2014a).

global ring system C1R+C2R, where W_i and p_{Ni} denote the physical width and normal opacity of each component, respectively. For a monolayer ring, W_e is a measure of the amount of material contained along a radial cut of that ring. It can be viewed as the width of an opaque monolayer ring that would block the same amount of light as the observed ring (see Elliot et al. 1984 and Chapter 4).

The fifteen or so C1R+C2R occultation profiles obtained so far provide a consistent value close to $W_{e(1+2)} \sim 2$ km (with typical dispersion of ~ 1 km), while the six profiles where C2R can be resolved from C1R provide $W_{e2} \sim 0.25$ km (with dispersion ~ 0.05 km), with no significant azimuthal variations. Thus, the system C1R+C2R does not show appreciable azimuthal variations in W_e and C2R appears to contain ~ 10 times less material than C1R.

7.2.2.3 Photometry

The long-term photometric evolution of Chariklo’s system is a natural consequence of the changing aspect of its rings. During the 63-years orbital period, the rings have an opening angle B to the Earth that varies between extreme values of about -60 to $+60$ degrees. Using the size, width and radius of Chariklo and its rings (Tables 7.1 and 7.2), it follows that the total apparent surface area of the rings at maximum B represents about 35% of Chariklo’s apparent surface area. For one of the possible ring pole positions previously discussed, the rings had their maximum opening angle in 1997 and were observed edge-on in 2008 (Fig. 7.4). The resulting changing apparent ring geometry then satisfactorily reproduces the shape and timing of Chariklo’s system absolute magnitude, while excluding the alternative solution aforementioned.

Elaborating on that, let us consider the photometric behavior of a flat, circular ring of radius a , width W and opening angle B . The brightness of such a flat surface is measured by its reflectivity I/F , where πF is the incident solar flux

density and I is the intensity emitted from the ring surface (remembering that the reflectivity of a perfect Lambert surface is $I/F = 1$). The flux densities F_r and F_C received from the main ring and Chariklo are respectively:

$$F_r \propto (I/F)_r S'_r \text{ and } F_C \propto p_C \phi_C(\alpha) S'_C, \quad (7.1)$$

where $S'_r = 2\pi a W \mu$ is the ring's apparent surface area, with $\mu = |\sin(B)|$, p_C is Chariklo's geometric albedo, α is the phase angle, $\phi_C(\alpha)$ is the phase function (with $\phi_C(0) = 1$ by definition), and $S'_C = \pi R_{\text{equiv}}^2$ is Chariklo's apparent surface area, where the equivalent radius R_{equiv} , see Table 7.1.

Defining H as the absolute magnitude of Chariklo's system (main body plus rings), i.e. its magnitude at 1 AU from Earth and Sun and at zero phase angle, and assuming that Chariklo's absolute magnitude H_C is essentially constant over time, we obtain:

$$10^{0.4(H_C - H)} = 1 + \frac{2aW\mu}{p_C \phi_C(\alpha) R_{\text{equiv}}^2} \left(\frac{I}{F} \right)_r \quad (7.2)$$

Monitoring of H vs. time (as μ changes) provides $(I/F)_r$, once Chariklo's photometric properties are known, as well as the parameters a and W , derived from occultation data (Table 7.2).

A more detailed modeling of the observed variations (Duffard et al. 2014a and Fig. 7.4) provides $(I/F)_r = 0.07 \pm 0.01$ at $0.55 \mu\text{m}$. We note that the reflectivity of Saturn's A ring, which has an optical depth comparable to that of ring C1R, is $(I/F)_{\text{ring A}} \sim 0.3$ (Hedman et al., 2013). Conversely, Uranus rings α and β , which also have optical depths comparable to that of C1R, have $(I/F)_{\alpha, \beta} \sim 0.05$ (Karkoschka, 2001). Thus, Chariklo's rings appear roughly three times darker than Saturn's A ring, twice as bright as Uranus' α and β rings, and about three times brighter than Chariklo's surface. Note also that at maximum opening angle ($B \sim 60^\circ$), the ring to Chariklo flux ratio is $F_r/F_C \sim 0.75$. In other words, the rings significantly contribute to the total flux received from the entire system.

7.2.2.4 Composition

The Chariklo system spectrum has been monitored since 1997, and also shows long-term variations. In particular, the water ice bands at $1.5 \mu\text{m}$ and $2 \mu\text{m}$ disappeared in 2007-08, while being prominent in 1997. The rings provide a natural explanation for that behavior: they contain water ice that vanished out of view during the 2008 ring plane crossing (Fig. 7.4).

By subtracting spectra when the rings are well open and spectra of Chariklo alone (edge-on geometry), one can obtain the spectrum of the rings alone, see Fig. 7.5. It clearly shows the presence of water ice, with a robustly derived abundance close to 20% (Duffard et al., 2014a). Other compounds must be present, but with far less constrained abundances, with degeneracies between the various species. Current estimates yield values of 40-70% silicates, 10-30% tholins and a small amount of amorphous carbon. Conversely, Chariklo's spectrum does not reveal any presence of water, and is consistent with about 60% of amorphous carbon, 30% of silicates and 10% of organics (Ibid.).

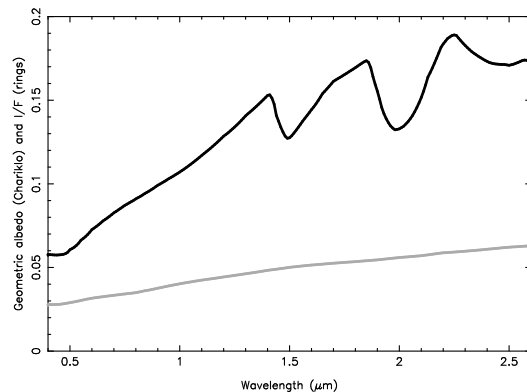


Figure 7.5 Synthetic spectra of Chariklo alone (gray) and its rings (black) derived from spectra of Chariklo's system obtained at different epochs, with various ring opening angles. This permits to disentangle the contributions from the main body and from the rings. Note the water ice bands around $1.5 \mu\text{m}$ and $2 \mu\text{m}$ in the ring spectrum. Adapted from Duffard et al. (2014a).

Of course, those spectra reveal surface properties, and may be unrelated to the bulk compositions of the ring particles and Chariklo's interior. In particular, they do not preclude the existence of water ice inside Chariklo.

7.2.2.5 Central body

Chariklo has a rotation period near 7 hours and an equivalent radius close to 120 km (Table 7.1). Unfortunately, other physical properties like size, shape or density are poorly constrained, while having important consequences on the ring dynamics, see the next subsection.

Currently, no direct imaging system can resolve Chariklo's disk (it subtends less than 0.03 arcsec on the sky), and there are not enough stellar occultations observed so far to pin down Chariklo's size and shape (which can be done in principle at kilometric accuracy using that method). The occultation data currently available show that Chariklo cannot be a spherical body. The observations are in fact consistent with either an oblate spheroid with equatorial and polar radii of 133×125 km, respectively, or an ellipsoid with main axes $167 \times 133 \times 86$ km, with typical uncertainties of 5 km on each dimension (Leiva et al. 2016, in preparation). Assuming a homogeneous body in hydrostatic equilibrium, this would imply densities of some $1\text{-}3 \text{ g cm}^{-3}$ (Maclaurin spheroid case) or close to 0.8 g cm^{-3} (Jacobi ellipsoid case), with corresponding dynamical oblatenesses around 0.07 and 0.20, respectively. Taken together, the two cases considered here imply a Chariklo mass in the range $0.6 - 3 \times 10^{19}$ kg.

It should be remembered, however, that an irregular shape cannot be currently discarded, and that the hydrostatic and homogeneous hypotheses may be invalid. Clearly, more multi-chord occultations are needed to build a correct model for Chariklo's size and shape.

7.2.3 Dynamics

7.2.3.1 Roche zone

Chariklo's tidal disruptive forces must be strong enough to prevent the accretion of ring particles into small satellites. To be disrupted, a particle at distance a from Chariklo should have a density ρ of the order of, or lower than a critical density ρ_{crit} (Tiscareno et al., 2013):

$$\rho < \rho_{\text{crit}} = \frac{4\pi\rho_C}{\gamma} \left(\frac{R_{\text{equat}}}{a} \right)^3, \quad (7.3)$$

where ρ_C and R_{equat} are Chariklo's density and equatorial radius, while γ is a dimensionless parameter that describes the structure of the disrupted particles. For instance, $\gamma = 4\pi/3$ for a sphere (see e.g. Murray and Dermott 1999), $\gamma \sim 1.6$ for a body that uniformly spreads into its lemon-shaped Roche lobe (Porco et al., 2007), and $\gamma \sim 0.85$ for the (unlikely) incompressible fluid case that corresponds to the classical Roche limit.

All the parameters in Eq. 7.3 are largely unknown. The occultation chords obtained in 2013 suggest that Chariklo is elongated, with $R_{\text{equat}} \sim 150$ km (see above). Moreover, values of $\gamma \sim 1.6$ seem the most appropriate in the context of planetary rings (Tiscareno et al., 2013). Taking $a \sim 400$ km, we obtain $\rho_{\text{crit}} \sim 0.4\rho_C$. For an expected icy body like Chariklo, we can assume $\rho_C \sim 1 \text{ g cm}^{-3}$. This suggests that the ring particles should be rather underdense ($\lesssim 0.5 \text{ g cm}^{-3}$) to prevent accretion. Such densities are actually typical of what is observed in the outer regions of Saturn's A ring (Tiscareno, 2013). As previously noted, however, while water ice is clearly identified in Chariklo's rings (Fig. 7.5), other compounds must be present, like silicates or tholins. This would make Chariklo's ring quite different, in terms of composition, from those of Saturn, which are basically pure water ice (see Chapter 3 by Cuzzi *et al.*). Very little is known about the physical properties of individual ring particles in general (including those of Saturn's rings). In that context, it remains to be seen if particles partly composed of silicates or tholins may have densities as low as 0.5 g cm^{-3} , for instance if they are porous or fluffy. Moreover, the criterion proposed in Eq. 7.3 might miss some of the physics at work and be too crude for a firm claim that Chariklo's ring particles must be underdense.

7.2.3.2 Local velocity field and thickness

Although hugely different in terms of size and mass, Chariklo's rings share a local velocity field similar to those of Saturn or Uranus. Using a typical mass $M_C \sim 10^{19}$ kg for Chariklo (see above), we obtain a ring orbital mean motion of $n \sim \sqrt{GM_C/a^3} \sim 10^{-4} \text{ s}^{-1}$ at $a \sim 400$ km, where G is the gravitational constant. This is comparable to the orbital motions in Uranus' rings and the outer part of Saturn's rings. Consequently, the local Keplerian shears, $dv/da = -3n/2$ (where v is the orbital velocity), are also comparable. In other words, a particle in Chariklo's rings essentially "sees" the same local velocity field as a particle in Saturn's and Uranus' rings.

In fact, the mere requirement that the rings must reside inside the Roche zone imposes the value of n , and thus of dv/da . In effect, combining Eq. 7.3 and $n = \sqrt{GM_C/a^3}$, we obtain $n \sim \sqrt{\gamma G \rho_{\text{crit}}/3}$. So, the velocity field surrounding the ring particles depends only on their physical properties, i.e. γ and ρ_{crit} , whatever the central body mass or the ring dimension are.

In the same vein, we see that the ring thickness h only depends on the particle physical properties, and not on the macroscopic ring parameters. A dense collisional ring tends to adjust itself so that its Toomre's stability parameter Q stays near unity:

$$Q = \frac{v_{\text{rms}} n}{\pi G \Sigma} \sim \frac{h n^2}{\pi G \Sigma} \sim 1, \quad (7.4)$$

where Σ is the ring surface density, v_{rms} is the ring particle velocity dispersion and h is the ring thickness, $h \sim v_{\text{rms}}/n$. As Chariklo's main ring is densely packed with particles, $\Sigma \sim \rho_{\text{crit}} R$, where R is the radius of the largest particles. So, $h \sim (3\pi)/\gamma Q R \sim$ a few times R from the estimation of γ given before, and from $Q \sim 1$. In the case of Saturn's rings, $R \sim 1$ m, so that $h \sim 10$ m (Colwell et al., 2009). We do not know the size distribution in Chariklo's rings, but if it is similar to that in Saturn's rings, they should also have a thickness of $h \sim 10$ m.

7.2.3.3 Mass and angular momentum

Only rough estimations of the ring mass and angular momentum can be made at the present stage. As argued in the previous subsection, the local kinematic conditions in the ring C1R should be close to those prevailing in Saturn's rings. Assuming a surface density $\Sigma \sim 500\text{-}1000 \text{ kg m}^{-2}$ for C1R (typical of Saturn's ring densest parts, Colwell et al. 2009), and considering the quantities in Table 7.2, we obtain a ring mass estimate $M_r \sim 10^{13}$ kg, equivalent to an icy body of radius ~ 1 km. This corresponds to a very small fraction of Chariklo's mass, $M_r/M_C \sim 10^{-6}$, and is larger than, but still comparable to the corresponding fraction in the case of Saturn's rings, $M_r/M_S \sim 10^{-7}$ (Cuzzi et al., 2009).

Another method can be used to estimate C1R's mass. Its physical width W varies from about 5.5 to 7.1 km (Table 7.2). This suggests that C1R may behave like some of the Uranian rings (French et al., 1991), i.e. a set of nested elliptical streamlines locked into a common precession rate regime, against the differential precession (stemming from the central body's oblateness) that should destroy this configuration.

In those models, the narrow ring is globally described by an ellipse with mean semi-major axis a and mean eccentricity e , while its inner and outer edges are described by aligned ellipses with semi-major axes a_{inn} and a_{out} , and eccentricities e_{inn} and e_{out} , respectively. To first order in e , the width of the ring then varies with true anomaly f as $W = \Delta a [1 - q_e \cos(f)]$, where $q_e = e + a \partial e / \partial a$ is a dimensionless parameter that depends on both the eccentricity and its gradient across the ring, $\partial e / \partial a = \Delta e / \Delta a$, with $\Delta e = e_{\text{out}} - e_{\text{inn}}$ and $\Delta a = a_{\text{out}} - a_{\text{inn}}$.

One mechanism proposed by Goldreich and Tremaine (1979b,a) to lock the streamlines into a rigid precession regime is self-gravity. In essence, the mass of the inner half of the ring increases the precession rate of the outer half, and vice-versa, thus maintaining the alignment. This requires a ratio M_r/M_C of the order of $(e/\Delta e)(\Delta a/a)^3 J_2(R_C/a)^2$, where J_2 is the dynamical oblateness of the central body. Elaborating on that basis, Pan and Wu (2016) estimate a C1R mass of a few 10^{13} kg, comparable to the estimate already given before. This reinforces the notion that the ring C1R is comparable, both in terms of surface density and dynamical behavior, to some of the dense and narrow rings of Saturn or Uranus.

Those estimates must be considered with caution, though, first because neither e nor q_e are currently known. The occultation data are not yet accurate and numerous enough to provide detailed ring orbital solutions and edge models.

Secondly, only variations of width W with respect to the *inertial* mean longitude λ have been derived right now, while variations vs. true anomaly f should be determined to test rigid precession models. This will be possible only when the ring apsidal precession rate $\dot{\varpi} \sim 1.5(R_C/a)^2 J_2 n$ is determined. An expected value of J_2 is $\sim \Omega_C^2 R_C^3 / 2GM_C$, assuming a homogeneous body, where $\Omega_C = 2\pi/P_C$ is Chariklo's spin rate. From Table 7.1, one obtains $J_2 \sim 0.08$ and $\dot{\varpi} \sim 10^{-6} \text{ s}^{-1}$, so that the ring apse should precess over a period of a couple of months only. This is much shorter than the eleven months or so separating the June 2013 and April 2014 occultations from which values of W are derived (Table 7.2). Consequently, it is not yet possible to compare consistently those observations and obtain a coherent plot of W vs. f .

Finally, we do not know yet if the observed width variation is caused by a $m=1$ azimuthal wavenumber, or by some higher (free or forced) wavenumbers which would require a revision of the mass estimation made above.

More generally, the physics at work in dense narrow rings may be more complex than the purely self-gravitating models evoked so far. In particular, viscous effects due to interparticle collisions near sharp ring edges resonantly perturbed by (yet to be discovered) shepherd satellites may significantly increase the mass estimation quoted above, see Chiang and Goldreich (2000) and Mosqueira and Estrada (2002). Those models predict enhanced ring surface densities at some 100-500 m from the edges, consistent with the double-dip structures observed in α and ϵ Uranus' rings occultation profiles (French et al., 1991), and interestingly, in the C1R profile too (Fig. 7.3).

Finally, approximating Chariklo as a homogeneous sphere of radius R_{equiv} , the ratio of the ring angular momentum to that of Chariklo is $H_r/H_C \sim (M_r/M_C)P_C\sqrt{G\rho_C}\sqrt{a/R_{\text{equiv}}}$. From Tables 7.1 and 7.2, we obtain $H_r/H_C \sim 10^{-5}$. Applying the same calculation to Saturn's rings, where we assume that the rings are uniformly spread between $\sim 92,000$ and $137,000$ km, we obtain a ratio $H_r/H_S \sim 10^{-6}$ (using $M_r/M_S \sim 10^{-7}$, see above). This is smaller than, but still comparable to the fraction H_r/H_C . In any case, we see that very small fractions of

Chariklo's mass and angular momentum are stored in the rings, a noteworthy result when it comes to discussing the rings' origin.

7.2.3.4 Putative shepherd satellites

Rings C1R and C2R are both sharply confined, see Fig. 7.3. If unperturbed, they should spread out on a timescale of (Goldreich and Tremaine, 1979b):

$$t_\nu \sim \frac{W^2}{\nu}, \quad (7.5)$$

where ν is the kinematic viscosity associated with particle collisions. A typical value of ν is $\sim nh^2$, where h is the ring thickness. Taking $W \sim 5$ km (Table 7.2), we obtain $t_\nu \sim 10^4/h^2$ years, where h is expressed in meters. Assuming again $h \sim 10$ m, we obtain $t_\nu \sim$ a few thousand years. Moreover, Poynting-Robertson (PR) differential drag also causes a spreading over a timescale of (Goldreich and Tremaine, 1979b):

$$t_{PR} \sim \left(\frac{c^2}{4f_\odot}\right) \left(\frac{W}{a}\right) \rho\tau R, \quad (7.6)$$

where c is the velocity of light, f_\odot is the solar flux density at Chariklo, ρ the density of the particles and τ is the optical depth. Taking $\rho < \rho_{\text{crit}} \sim 0.5 \text{ g cm}^{-3}$, as explained before, and $\tau \sim 1$, we obtain a typical value of $t_{PR} \sim 10^9 R_{\text{meters}}$ years, i.e. a few million years for sub-cm particles. The effect of PR drag is even more drastic for smaller grains, with a depletion time of only a few months for micrometric particles. Even if very crude, these estimations show that Chariklo's rings are either very young, or confined by an active mechanism.

It is remarkable that apparently similar ring confinement occurs in systems so widely different (in terms of orbital radii) as those of Saturn or Uranus, compared to Chariklo. In fact, looking at Chariklo's rings' optical depth profiles (Fig. 7.3), it is hard to distinguish them from their Uranian cousins, see French et al. (1991) and Chapter 4.

A classical theory to confine ring material invokes the presence of putative "shepherd satellites". In its simplest version, a shepherd of mass M_s can exert a torque T_m onto a ring edge at a discrete $m+1 : m$ mean motion resonance (where the ring particle completes $m+1$ revolutions while the satellite completes m revolutions, with m integer), see Goldreich and Tremaine (1982):

$$T_m \sim 8.5m^2 a^4 n^2 \Sigma \left(\frac{M_s}{M_C}\right)^2. \quad (7.7)$$

As m increases, resonances overlap and the torque density (torque per unit interval of semi-major axis) is:

$$\frac{dT}{da} \sim 2.5a^3 n^2 \Sigma \left(\frac{M_s}{M_C}\right)^2 \left(\frac{a}{x}\right)^4, \quad (7.8)$$

where x is the distance between the satellite and the ring. To prevent spreading, the satellite torque must balance the viscous torque T_ν associated with inter-particle collisions. In a Keplerian velocity field, it is:

$$T_\nu = 3\pi n a^2 \nu \Sigma. \quad (7.9)$$

Making $T_m = T_\nu$, and in the case of discrete resonances, the radius R_s of a shepherd with density ρ_s is:

$$R_s \sim \left(\frac{\rho_C}{\rho_s}\right)^{1/3} \left(\frac{h}{ma}\right)^{1/3} R_C. \quad (7.10)$$

This yields radii of a few km for icy shepherds ($\rho_s \sim 1 \text{ g cm}^{-3}$), taking m of a few times unity and h a few meters. Concerning the gap between C1R and C2R, it should be opened in the overlapping resonance regime (Eq. 7.8), in which case, the radius of the satellite is (Goldreich and Tremaine, 1982):

$$\frac{R_s}{R_C} \sim \left(\frac{\rho_C}{\rho_s}\right)^{1/3} \left(\frac{h}{a}\right)^{1/3} \left(\frac{W_{\text{gap}}}{a}\right)^{1/2} \lesssim 1 \text{ km} \quad (7.11)$$

where $W_{\text{gap}} \sim 8.5 \text{ km}$ is the full width of the gap (Table 7.2). Note in passing that the mass of the shepherds estimated here would be comparable to that of the rings (see the previous subsection). In other words, there would be roughly the same amount of material in the form of rings and in the form of (putative) shepherd satellites.

This said, this model poses new problems. In effect, as the shepherd confines a ring through a torque T_m , the reaction from the latter induces a migration rate $|\dot{a}_s| \sim 2|T_m|/(anM_s)$, where a_s is the shepherd's semi-major axis. Considering that $T_m = T_\nu$ and using Toomre's criterion of Eq. 7.4, one obtains:

$$|\dot{a}_s| \sim 36m \left(\frac{h}{a}\right) \left(\frac{h}{T_{\text{orb}}}\right), \quad (7.12)$$

where T_{orb} is the orbital period. We may apply this formula to the shepherd satellites Cordelia and Ophelia which confine the Uranian ϵ ring. In this case, $m \sim 10$, $T_{\text{orb}} \sim 10$ hours, $a \sim 50,000 \text{ km}$ and $h \sim 10$ meters. This yields $|\dot{a}_s| \sim 1 \text{ m s}^{-1}$. As the shepherds orbit at some 1000-2000 km from the ϵ ring, this implies short recession timescales of some million years for those two satellites. This problem is exacerbated for Chariklo, due to the smallness of the semi-major axis a (by more than two orders of magnitudes) compared to the case of the giant planets. Applying Eq. 7.12 to the Chariklo case actually provides recession timescales of some thousands of years only if one assumes again $h \sim 10$ meters, and considering that T_{orb} must again be of the order of 10 hours.

One possibility is that, for a so far unexplained reason, Chariklo's ring particles are much smaller than those of Saturn or Uranus, resulting in a much smaller value of h , and thus, much longer recession timescales for the shepherds. The shepherding physics may also be more complex than assumed here. For instance, the viscous torque (7.9) can be significantly reduced due to the local reversal of the viscous angular momentum flux, caused by the satellite itself (Goldreich and Porco, 1987). This in turn would reduce the masses of the shepherds estimated above, as well as their migration rates.

In summary, and except if Chariklo's rings are very young, some deep understanding of the shepherding mechanism, and in particular a better knowledge of the ring local collisional dynamics are required to better assess the short

timescale problems described above. In that context, detections of the putative shepherd satellites would be very helpful to understand Chariklo's ring confinement, but this remains a very challenging observational task.

At this point, it is worth mentioning that resonances may arise not from satellites, but from the very shape of Chariklo. For instance, a topographic feature of some 5 km in height on Chariklo's surface might cause (tesseral-type) resonant perturbations that are comparable in strength to those stemming from the putative satellites mentioned above. The same is true if the body is elongated in one direction by a few kilometers, in which case non-axisymmetric perturbations arise from the bulges associated with the elongation. Assuming that Chariklo's mass is in the range $0.6 - 3 \times 10^{19} \text{ kg}$, the corotation radius – where particles have an orbital period matching that of Chariklo ($\sim 7 \text{ h}$) – would lie somewhere between 185 and 320 km. On each side of this corotation radius, first order commensurabilities $m + 1 : m$ between the particle mean motion and Chariklo's orbital period would appear. It is instructive to note that the 2/1 outer resonance (corresponding to particles with orbital period close to 14 h) should occur somewhere between 290 and 510 km, bracketing the region where the rings are found. It is too early to conclude anything before accurate measurements of Chariklo's mass and shape are made, but it is worth remembering that the ring dynamics might be significantly influenced by resonances with the spin of the central body.

7.2.4 The origin of Chariklo's rings

The general portrait that emerges from the previous subsections is that of a ring system composed of underdense particles ($\rho \lesssim 0.5 \text{ g cm}^{-3}$), partially composed of water ice, and confined by small shepherd satellites of some kilometers in size that contain a mass comparable to that of the rings. Moreover, a very small fraction of mass ($\sim 10^{-6}$) and angular momentum ($\sim 10^{-5}$), compared to Chariklo, are required to explain the observed rings.

7.2.4.1 Rings around other small bodies

At present, it remains unclear whether Chariklo's rings are generic and frequent features around small bodies, or are an exceptional system resulting from a fine tuning between various physical properties. Hundreds of Main Belt asteroid occultations have been monitored, but no report of secondary events possibly due to rings have been reported so far. A handful of occultation events involving TNO's have been published up to now (Elliot et al., 2010; Sicardy et al., 2011; Ortiz et al., 2012; Braga-Ribas et al., 2013), and again no evidence of ring events have been documented. It should be noted, however, that Chariklo's rings cause very brief stellar drops (at sub-second level, see Fig. 7.2) that are easily overlooked if integration times and/or noise levels are too large. Also, re-analysis of the best occultation data sets obtained so far might reveal ring-related features. Moreover, imaging such systems is challenging from Earth. For instance, Chariklo's rings do not span more than 0.04 arcsec around the main body. This makes direct detection very hard, even

on the best instruments available nowadays. So, other ring systems may still be undiscovered due to the lack of high-quality occultation observations or high resolution imagers.

7.2.4.2 The case of Chiron

The object (2060) Chiron is the second largest Centaur known to date, with a diameter of 218 ± 20 km (Fornasier et al., 2013) and perihelion-aphelion distances of 8.4-18.8 AU. Two stellar occultations observed in 1993 and 1994 actually revealed secondary events that were interpreted as due to collimated cometary jets (Elliot et al., 1995; Bus et al., 1996). A more recent Chiron occultation in 2011 revealed symmetric, narrow and sharp double dips, similar in depth and width to those observed around Chariklo. They have been interpreted as being due to a spherical shell surrounding Chiron (Ruprecht et al., 2015) or to a ring system akin to those of Chariklo.

The ring hypothesis is supported by various arguments (Ortiz et al., 2015): (1) the strong similarity between the event reported by Ruprecht et al. (2015) and the one in Fig. 7.2, (2) the fact that the reconstructed ring orientation globally explains the photometric behavior of Chiron since ~ 1980 , with a minimum in 2001 when the rings should be observed edge-on, (3) the fact that this also explains the variations over time of Chiron's rotational lightcurve amplitude, assuming that the rings lie in the equatorial plane of a tri-axial central body, and (4) the fact that Chiron's spectrum exhibits variations of the water ice band, with a disappearance in 2001 that would be caused by an edge-on geometry of the ring at that epoch, as it is the case for Chariklo in 2008. However, the ring hypothesis remains debatable as Chiron has cometary activity (Meech and Belton, 1989; Luu and Jewitt, 1990) that may skew the interpretation. Moreover, the 1994 Chiron occultation showed one sharp secondary event followed by a more diffuse stellar drop that is incompatible with azimuthally uniform narrow and dense rings, perhaps calling for the existence of incomplete rings (arcs) instead. Discriminating between the shell and ring interpretations (or others) clearly requires higher-quality multi-chords occultations.

In any case, it is interesting to see that Chiron, a Centaur similar to Chariklo in terms of size and orbit, is also surrounded by optically dense material. This suggests that common physical processes may be at work, giving rise to unaccreted closeby material.

7.2.4.3 Are Centaurs special?

Several circumstances can make Chariklo (and possibly other Centaurs) special to allow it to possess rings: (i) its heliocentric distance, (ii) possible transient cometary activity, (iii) its size, and (iv) significant gravitational perturbations from the giant planets.

Point (i) is discussed by Hedman (2015), who considers that water ice particles may have the adequate physical properties to meet the condition given in Eq. 7.3 between 8 and 20 AU. More precisely, in that heliocentric range, water ice may reach a typical temperature of 70 K, low enough for

the ice to avoid sublimation (which explains why no rings are seen around Main Belt asteroids), but still high enough to remain weak and consequently be subjected to tidal disruption in the Roche zone. This would be consistent with the fact that Chariklo travels between 13 and 19 AU from the Sun.

Another circumstance linked to heliocentric distance is the lower impact velocities prevailing in Chariklo's region - typically 1 km s^{-1} - compared to relative velocities in the Main Belt, about 5 km s^{-1} . This results in much less destructive collisions that may give rise to a debris disk around the impacted body, from which rings form, instead of dispersing most of the pieces to infinity.

Turning to point (ii), it appears that some Centaurs have cometary activity. This is documented for Chiron (Meech and Belton, 1989; Luu and Jewitt, 1990) and Echeclus (Rousselot, 2008), a Centaur with perihelion-aphelion distances of 5.8-15.6 AU and diameter of about 65 km (Duffard et al., 2014b). In Echeclus' case, the cometary-like episode of March 2006 showed a coma around a source that was *separated* from Echeclus. This coma may have been caused by a 8-km object moving near the main body, that could be a satellite or a fragment ejected from the surface. This adds one case in the list of Centaurs surrounded by (in this case, transient) material.

The escape velocity at the surface of a body of density ρ and radius R is

$$v_{\text{esc}} = \sqrt{\frac{8\pi G\rho}{3}} R \sim 0.75 R_{\text{km}} \text{ m s}^{-1}, \quad (7.13)$$

assuming an icy body ($\rho \sim 1 \text{ g cm}^{-3}$). This implies a rough value of $v_{\text{esc}} \sim 100 \text{ m s}^{-1}$ for Chariklo or Chiron. This is typical of the upper limit for terminal velocities of dust grains in a cometary coma (Delsemme, 1982; Tenishev et al., 2011). This coincidence raises the interesting possibility that Chariklo's rings have an endogenous origin. They could be formed of cometary material ejected from the surface with velocities large enough to prevent an immediate in-fall onto the surface, as is the case for Triton's geyser material, but still small enough to prevent escape to infinity, as is the case for km-sized comets.

In any case, no dust production has been observed so far for Chariklo (Guilbert et al., 2009), with an upper limit of about 2.5 kg s^{-1} for the dust production rate (Fornasier et al., 2014). Similarly, no gas production has been found for that body, with typical upper limits of 2×10^{28} molecules s^{-1} of CO ($\sim 10^3 \text{ kg s}^{-1}$) and 8×10^{27} molecules s^{-1} of HCN ($\sim 400 \text{ kg s}^{-1}$), see Bockelée-Morvan et al. (2001). In that context, deeper searches for dust or gas production might reveal a low level cometary activity for Chariklo, and thus constrain ring origin models.

Finally, we already noted that Chariklo is moving on an unstable, short life-time (10 Myr) orbit controlled by Uranus (Horner et al., 2004). The encounter distance Δ_{disrupt} at which a ring of semi-major axis a is disrupted is given by the Hill sphere radius $\Delta_{\text{disrupt}} \sim a(3M_U/M_C)^{1/3}$, where M_U is the Uranus mass. Using $M_U \sim 10^{26} \text{ kg}$, $M_C \sim 10^{19} \text{ kg}$ and $a \sim 400 \text{ km}$ yields $\Delta_{\text{disrupt}} \sim 5$ Uranian radii. Current estimations show that such a small distance has a small prob-

ability to occur (some 10%, see Hyodo et al. 2016) during Chariklo’s migration, and that globally Chariklo’s ring system can survive more than 90% of its encounters with giant planets (Araujo et al., 2016). In other words, if Chariklo’s rings were already formed while the object was in the TNO region, they should have safely experienced the migration episode.

However, encounters with Uranus may have destabilized a pre-existing, marginally stable Chariklo’s *satellite* system, causing orbit crossing and then collisions between the satellites, resulting in ring formation, a scenario that is still to be investigated. Note finally that a mere disruption of Chariklo during a close encounter with Uranus may also be envisaged. This might result in a debris disk around the body, from which small moons shepherding ring material could emerge near Chariklo’s Roche limit (Hyodo et al., 2016).

7.3 Rings around natural satellites

Currently, no rings have been confirmed orbiting natural satellites in our solar system, but physical evidence suggests that such rings could have been a common occurrence in the past. In fact, equatorial features occur on two moons of Saturn, Rhea and Iapetus, and could be remnants of such rings, as discussed below.

7.3.1 Iapetus

The ridge on Iapetus is a puzzling feature, up to 20 km tall and about 100 km wide, see Denk et al. (2005a,b) and Fig. 7.6. It is challenging to reconcile this with the global history of Iapetus. One approach has modeled it as the outcome of endogenic (tectonic or other) processes, but none could satisfy the observational constraint of a single equatorial high-standing ridge, see Castillo-Rogez et al. (2007) and Robuchon et al. (2010). Alternately, an exogenous origin has been proposed - the remnants of a ring that has fallen to the surface (Ip 2006; Levison et al. 2011; Dombard et al. 2012). Following this latter idea, one can use the constraining observed features of the Iapetan ridge - its dimensions, morphology/slopes and some localised cases of parallel ridges or tracks - and combine them with the dynamics of the Saturnian system and a ring’s tidal evolution to estimate the origin and properties that this proposed ring could have had.

Note that the Voyager imaging had not high enough resolution at equatorial latitudes to detect directly any significant equatorial topography (Smith et al., 1981, 1982). However, the analysis of the limb data many years later strongly pointed to a massive mountain-like structure with heights up to 20 km (Denk et al., 2000). These were identified in the Cassini Regio (the dark leading side) between the longitudes of 180 W and 200 W.

The most significant imaging of the equatorial ridge was done by the Cassini spacecraft during a flyby on 31 December 2004. The dark, leading side, was reported by Porco et al. (2005) to have an equatorial ridge up to 20 km in height,

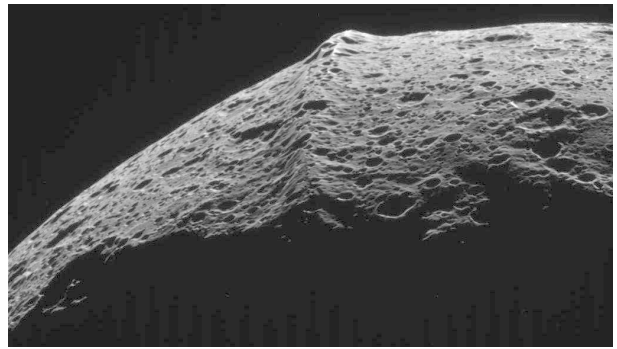


Figure 7.6 An image of the ridge of Iapetus taken from around 62,000 km in September 2007 by the Cassini-Huygens mission (image number N00091828; credit to NASA/JPL-Caltech/Space Science Institute).

confirming Denk’s finding. Profiles from the Digital Terrain Model (DTM) constructed from Cassini data find a diversity in the morphology of the ridge. At times it has a strictly steep-sided triangular shape (see ridge profiles r1 and r2 in Fig. 5 of Giese et al. 2008), while at others a more “flat-top” or trapezoidal shape characterized by lower slopes on the Northern side estimated to decrease to 15 deg down to 8 deg in ridge profile r3 and 4 deg in ridge profile r4. Subsequent global mapping of the topography (by PMS, published in Dombard et al., 2012) shows that the ridge is discontinuous with a series of linear ridges and isolated quasi-conical massifs along the equatorial trace. The elevation is variable along the length and appears to be absent in some stretches, though it is essentially global in character.

The trailing side DTM was constructed of only two sets of stereo pairs, but reveals that the ridge continues on the back hemisphere, and appears to be centered at 30 deg East (Giese et al., 2008). Given the current observations, with confirmed existence of the ridge spanning the entire well-observed leading side hemisphere (Porco et al., 2005; Giese et al., 2008), the leading side limb and also the trailing side (Giese et al., 2008) it is safe to assume that this feature is indeed global.

The size and the equatorial location of the ridge made it an enigmatic feature, but the larger context at Iapetus also includes its synchronous spin state, and its non-equilibrium global shape. Iapetus is synchronously locked with its orbital period around Saturn of 79 days, and estimates based on solid-body tides suggest that de-spinning to this state would take > 10 Gyr (Peale, 1977). Meanwhile, the global shape of Iapetus suggests it is not in hydrostatic equilibrium, as it has a shape expected for a body with a 16-h rotation rate (Thomas et al., 2007; Castillo-Rogez et al., 2007; Thomas, 2010). Combined, the features of the equatorial ridge and the spin state and global shape of the entire icy satellite point to a complicated history, one in which the ridge could have formed from an in-falling ring (Ip, 2006).

Two distinct takes on this idea have been explored. Levison et al. (2011) propose that Iapetus suffered a violent impact, and ejecta formed a large disk of debris that quickly damped to the equatorial plane straddling the synchronous

limit for a then-faster spinning Iapetus (as the global shape implies a faster rotation in its past) – similar to the proto-lunar disk at Earth. A sub-satellite forms from the disk beyond the Roche limit and the synchronous limit, and its tidal interactions with the remaining debris push the ring to the surface of Iapetus forming the equatorial ridge. The sub-satellite then tidally evolves away from Iapetus, slowing the rotation of Iapetus and aiding its de-spinning until it is eventually stripped from the orbit of Iapetus.

Dombard et al. (2012) propose a similar scenario, but with a different origin and fate for the formed sub-satellite. Here, a ~ 100 km body impacts Iapetus and is captured into orbit – similar to the Pluto-Charon formation scenario. If the orbit is retrograde it will tidally evolve inward until reaching the Roche limit, after which it will be tidally disrupted and eventually rain down to the surface piece by piece building the equatorial ridge.

While there are some differences in the models, they both propose the existence of a substantial ring orbiting Iapetus in its past. Fundamentally, both models would require a ring with a minimum mass equal to that needed to create the equatorial ridge. Estimates for this mass depend on the assumed shape and size of the ridge before its degradation due to bombardment over Solar System timescales - it has been estimated between 5.5×10^{17} and 4.4×10^{19} kg (Ip, 2006; Levison et al., 2011), or a fraction up to a few percent of the mass of Iapetus. The Levison et al. (2011) model would actually require more mass in the ring initially, as it would eventually build a sizable sub-satellite leaving behind enough mass in the ring to then fall to the surface and build the ridge.

Neither model predicts a long lifetime for the ring. Levison et al. (2011) find a spreading timescale of only 100's of years owing to the strong tidal interaction with the sub-satellite. Meanwhile, the timescale for the survival of a ring is longer in Dombard et al. (2012) as there is no external interaction with other orbiting debris - the sub-satellite is tidally disrupted and then falls piecewise onto the surface on tidal timescales. This was estimated to be quite rapid compared to the 10-100's Myr tidal timescales of the system, owing to the eventual ring having a very high surface mass density and therefore rapid viscous evolution. The timing of the formation, evolution and demise of the ring is different in each case as well. The ring in Levison et al. (2011) would form and be lost coincident with the large impact and birth of the sub-satellite, with a longer tidal scenario to play out with the sub-satellite. The Dombard et al. (2012) scenario would have the ring form well after the impact and tidal evolution of the sub-satellite, so at the end of the story. While these may not be testable distinctions for Iapetus with the current dataset, they do provide scenarios that could be distinguished in other parts of our Solar System or external to our Solar System.

While these are both compelling models, much of their viability lies in the geophysical evolution of Iapetus, the large uncertainties in tidal evolution timescales, and even in the impact physics of ring particles pummeling the surface. Further advances could be made by better understanding the

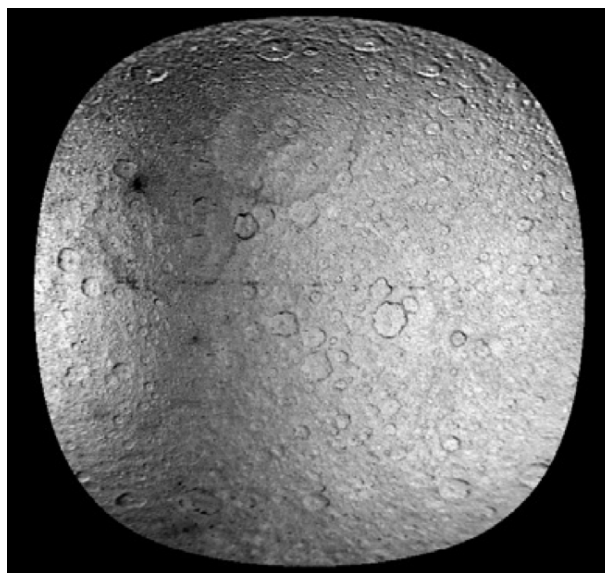


Figure 7.7 This view shows a Cassini color ratio map (IR3/UV3) of the anti-Saturnian facing hemisphere of Rhea. Such maps reveal discrete spots along the equator 20-50 km across that have unusual spectral signatures enhanced in the ultraviolet, giving them a “bluish” appearance in Cassini 3-color mosaics. Each spot correlates with local highs in topography. Effective resolution is ~ 1.75 km/pixel.

stratigraphy on the surface of Iapetus to date the ring and understand its relationship to some of the largest impacts.

7.3.2 Rhea

In 2009 a putative ring was reported in orbit around Rhea, after sharp drops in measured electron counts from the fields and particles instruments, symmetric about the moon, were detected by the charged-particle detectors aboard the Cassini spacecraft (Jones et al., 2008). However, deep searches in both high-phase and low-phase Cassini ISS narrow-angle camera images ruled out dust material orbiting Rhea as an explanation for those drops (Tiscareno et al., 2010). After this report, independent workers examining multispectral ISS mosaics of Rhea discovered “blue pearls” on the surface of that moon (Schenk et al. 2011). These features take the form of irregularly shaped surface patches 5-50 km wide and 50-150 km apart, visible only as color anomalies, and only along the equator of Rhea (Fig. 7.7). These patches are brighter in the near-UV and hence have a bluish signature when mapped in UV-green-IR filter combinations. The key observation at Rhea is that these spots or “Blue Pearls” form only on the highest local topography along the equator (Schenk et al., 2011), consistent with infalling orbiting debris striking the surface in the manner suggested by Ip (2006) for Iapetus. No constructional mountains or ridges are associated with these features, however, as the relief along the equator consists of pre-existing crater rims and ridges. The Schenk et al. (2011) proposal was that fine material spiraled in toward the surface and disturbed regolith on high topographic ridges. Due to the very low impact angles, lower lying topography “downstream” of these

impact points would be shielded from impact and thus uncolored.

7.3.3 Comparison of Iapetus and Rhea features

By itself, the equatorial ridge on Iapetus remained enigmatic, though all efforts to identify a tectonic mechanism failed. The discovery of a second non-tectonic equatorial feature on Rhea strengthens the case for ring deposition. The major difference at Rhea (compared to Iapetus) is that there is no significant accumulation of a topographic deposit at Rhea, suggesting that the mass of the ring system there was also much less than at Iapetus.

This said, two major features link the Rhea Blue Pearls and the Iapetus ridge. The first is the narrow equatorial great circle pattern of both. The second is the discontinuous nature of both. The Blue Pearls are widely separated and occur only on high-standing topography. The Iapetus ridge is also discontinuous and forms widely separated sub-ridges and promontories along the equator (Fig. 7.6s). In the case of a low-mass ring system, only the tops of high-standing features crossing the equator would be disturbed by infalling debris (as at Rhea). In the case of a massive ring system, material would accrete “backwards” along the equator at high standing blocking ridges, forming a partial ridge. With enough mass, a more continuous ridge is built up.

The two moon putative ring deposits appear to be of different ages. The Rhea color anomaly is a surficial effect and easily erased. The inference is that it is not ancient as blue color signatures fade over time and are not visible in older eroded craters. The small-scale complexity of these spots also points to a relatively young age as small scale features always tend to be ground up into the regolith of airless planetary bodies within a billion years or so, depending on location. The Iapetus ridge is much more massive and not easily destroyed or eroded. Landslides have affected its profile (Singer et al., 2013) and it is heavily cratered. Some large craters cut into it. It is inferred that it is very ancient, but also it does not appear to be primordial as its profile would be much more dissected than it appears. We infer that it formed sometime within the first 1-2 Gyr of formation but that tighter constraints on age are lacking.

Finally, no equatorial features (ridge, color anomaly, or otherwise) have been observed on other icy moons of Saturn, while mapping on the Uranian satellites is limited by poor coverage of the equatorial regions. Color and topographic mapping are at least as good on the other Saturnian satellites as they are on Rhea and Iapetus, and if such ring deposits ever formed they have either been erased by subsequent bombardment or E-ring deposition (e.g., Schenk et al., 2011) or never formed. The surficial Rhea Blue Pearls are easily erased over time, and are therefore geologically recent, but the apparent great age of the Iapetus ridge is such that large massive ring deposits of this kind would have been preserved through much of Saturn System history. The lack of prominent ridges on other Saturnian satellites is thus real and indicates that if any formed at those bodies, they formed very early and were erased in the accretional storm of projectile bombardment.

7.3.4 Rings around Uranian moons

Finally, the case for rings or ridges associated with the Uranian moons is not clear, namely because Voyager lacked the color filters that Cassini observed the Rhea ring deposit with, but also because the 1986 Uranus encounter provided our only mapping to date. Like Voyager at Saturn, these maps are incomplete, and provided imaging on the outer Uranian satellites Titania and Oberon (where rings are likely to be more stable) at no better than 2 to 5 km/pixel, respectively, and only of the southern hemispheres. Thus it is likely that both Blue Pearls and an equatorial ridge on one or more of these moons were missed by Voyager, if they exist. A return to the Uranian system will be required to determine if moon-rings ever formed there.

7.4 Rings around Mars

Studies of the giant planets have revealed a distinct connection between small moons and dusty rings (see Chapter 13). The concept is simple—meteoroids impact the surface of a moon and raise a cloud of dust. That dust escapes from the moon’s weak gravity but remains in orbit around the central planet. For example, Jupiter’s gossamer rings are associated with Amalthea and Thebe (Burns et al., 1999). Similar rings emerge from several small satellites of Saturn (e.g., Pan, Anthe, Aegaeon and Phoebe), Uranus (Mab) and Neptune (Galatea). In an analogous way, we would expect impacts into Phobos and Deimos to populate faint Martian dust rings. Soter (1971) was the first to predict the existence of rings of Mars, using a similar argument. Since then, the hypothetical Martian rings have been the topic of over thirty theoretical publications; see Krivov and Hamilton (1997) for a historical summary.

Dynamical simulations by Krivov and Hamilton (1997), building upon previous work (Juhasz and Horanyi, 1995; Krivov and Titov, 1995; Ishimoto, 1996), indicate that the Martian rings will have some peculiar properties. Because of the strong influence of solar radiation pressure, both rings are offset from the center of the planet, with the Phobos ring displaced toward the Sun by \sim one Martian radius, whereas the Deimos ring should be displaced away from the Sun by several radii. This peculiar result follows from the dynamics of individual dust grains. Briefly, Mars’ oblateness causes elliptical orbits of Phobos’ ring particles to precess faster than Mars’ mean motion around the Sun, whereas for Deimos, this precession is slower than Mars’ mean motion. Solar radiation pressure, which drives orbital eccentricities, is very sensitive to the difference between the two motions; the results are rings offset in opposite directions. The Phobos ring should be equatorial and \sim 400 km thick. The Deimos ring is predicted to be much thicker, 10,000–15,000 km, and tilted out of the equatorial plane toward the ecliptic by $\sim 15^\circ$. The larger thickness and tilt are both due to solar radiation pressure, which is a more effective perturbation for this more distant ring. Similar solar perturbations are responsible for the warps in Saturn’s E ring, and for the tilt and thickness

of the Phoebe ring (see Chapter 13). Also, the strong solar radiation pressure quickly drives micron-sized grains out of orbit, by inducing eccentricities large enough that they strike the planet; this leaves behind a ring that should be composed primarily of particles tens of microns or larger (Hamilton, 1996; Krivov and Hamilton, 1997).

So far, attempts to observe rings around Mars have been unsuccessful. Duxbury and Ocampo (1988) used Viking images to put an upper limit on the ring's normal optical depth $\tau < 3 \times 10^{-5}$. *In situ* observations by Mars-orbiting spacecraft of anomalies in the solar wind magnetic field were interpreted in the 1980s as being due to Martian rings, but more extensive measurements by the magnetometer aboard *Mars Global Surveyor* showed that observable fluctuations are likely due to well-known solar wind or bowshock phenomena (Øieroset et al., 2010).

Earth-based, telescopic detection of rings around Mars is more difficult than for analogous rings of the gas giants, because of the former's lack of atmospheric methane. Methane has very strong absorption bands at, e.g., $2.2 \mu\text{m}$, so the brightness of the giant planets drops substantially at selected wavelengths, facilitating the detection of faint rings. Mars has no analogous absorption bands. Nevertheless, the Hubble Space Telescope (HST) has been used four times to search for Martian rings. Two early attempts (HST programs GO-5493 and GTO-7176) used inappropriate viewing geometries and did not succeed; these results are unpublished. On May 28, 2001, Mars' hypothetical ring plane appeared edge-on to Earth within weeks of its opposition, providing the best Earth-based opportunity to detect these rings for several decades. Using the Wide Field/Planetary Camera 2 (WFPC2), Showalter et al. (2006) obtained upper limits of $\tau < 3 \times 10^{-8}$ for the Phobos ring and $\tau < 10^{-7}$ for the Deimos ring. This limit was sufficient to rule out rings at the upper end of the dust density predictions by Krivov and Hamilton (1997). A final attempt with HST, by the same team, employed a slightly inferior viewing opportunity in December 2007. Using the finer sensitivity of the Advanced Camera for Surveys (ACS), the observing plan had the potential to detect rings 30–100 times fainter than the previous limit. However, due to the failure of the ACS prior to the observations, the system was again imaged using WFPC2 and the ring detection threshold could not be improved.

Despite the lack of detections, the dynamics of dust in the Martian environment is well understood, and there remains little doubt that dust rings, at some very low level, must be present. The most plausible remaining method for detecting them would entail placing a sensitive dust detector into orbit around Mars. Japan's Nozomi spacecraft did carry such an instrument, but it failed to enter orbit around Mars in 1999 as planned. Perhaps some future Mars mission will finally reveal these long-sought rings.

7.5 Rings around Pluto

The discoveries of Pluto's small moons Nix and Hydra in 2005 (Weaver et al., 2006) raised the possibility that it, like

Mars, could harbor a tenuous ring system. Charon is less likely to be a major source of dusty rings because its gravitational field will more efficiently retain any dust ejected from its surface. Using the discovery images from HST, Steffl and Stern (2007) searched for rings in the orbits of the two small moons. They obtained upper limits of a few $\times 10^{-7}$ in reflectivity which, depending on the rings' albedos, corresponds to $\tau \lesssim 10^{-6}$. This is comparable to the conservatively estimated $\tau < 10^{-6}$ suggested by Stern et al. (2006).

The limiting factor in the search by Steffl and Stern (2007) was the extensive glare from Pluto and Charon. Showalter et al. (2011) used an alternative technique with HST to control for and subtract the glare pattern, making a more sensitive ring search possible. That program did not detect any rings, setting a new upper limit of $\tau < \text{a few } \times 10^{-7}$. However, it did reveal a fourth moon, Kerberos. The following year, a more extensive HST observing program revealed a fifth moon, Styx (Showalter et al., 2012).

With New Horizons en route to its July 2015 flyby of Pluto, the revelation of such an extensive satellite system raised concerns about a possible dust hazard to the spacecraft. However, dynamical studies in advance of the flyby tended to minimize that risk. Showalter and Hamilton (2015) showed that the satellite system is on the edge of chaos, which reduces the likelihood of a stable ring system. Porter and Stern (2015) showed that relatively few stable orbits exist between the four small outer moons, and those that do exist require a nonzero inclination. Furthermore, it had been noted that, somewhat counterintuitively, solar radiation pressure is an important consideration in the Pluto system because, although the Sun is very far away, Pluto's gravity is also quite weak.

Showalter and Hamilton (2010) showed that micron-size grains are quickly driven into orbits that collide with Charon, leaving behind particles primarily larger than $\sim 25 \mu\text{m}$. More detailed models showed that Nix and Hydra should be the main dust provider for broad and tenuous rings through micrometeoroid impacts. Combined effects of radiation pressure, collisions of the ejecta with the larger bodies Pluto and Charon and escape, however, seriously limit the optical depth of such rings. Poppe and Horányi (2011) estimated optical depths on the order of 10^{-7} for grains between 0.1 and $100 \mu\text{m}$ in size. On the other hand, Pires dos Santos et al. (2013) showed that radiation pressure remove very rapidly (on year-scales) particles with sizes around $1 \mu\text{m}$, leaving rings with normal optical depth on the order of 10^{-11} .

An extensive survey of the Pluto system was conducted throughout the New Horizons mission approach phase. No new moons and no rings were detected, and the spacecraft passed through the system safely. The final upper limit on the dust optical depth was 10^{-7} (Spencer et al., 2015). After the flyby, the spacecraft conducted an outbound search for faint rings at high phase angles. However, the analysis of that data set is still underway and no results have been reported.

Stellar occultations also provide an opportunity to search for rings. Optically thin rings would be generally undetectable by this method, but rings that are narrow and/or

dark could potentially show up in occultations before they are imaged directly. Historically, this is how the rings of Uranus and the arcs of Neptune were discovered. Boissel et al. (2014) conducted one such search, setting an upper limit of 30–100 m for the equivalent depth of a narrow ring (see Chapter 4 for the formal definition of “equivalent depth,” a form of radially-integrated optical depth). Similarly, Throop et al. (2015) set a limit of ~ 170 m assuming a nominal ring of width 2.4 km.

7.6 Rings around exoplanets

Studies of transient photometric changes have predominantly focused on objects that brighten, such as novae or gravitationally micro-lensed objects. The exceptions to this rule are the recent searches for exoplanet transits that find periodic but shallow and short dimming events. Thousands of exoplanets have been discovered using transit searches, however, with one exception, J1407 (Kenworthy and Mamajek, 2015), these have not been interpreted in terms of exoplanetary ring systems. Detection algorithms that rely on periodicity, fitting a known transit shape to the dimming event or that ignore deep events from eclipsing binaries would likely discard an eclipse from a circumsecondary and circumplanetary disk (Mamajek et al., 2012; Meng et al., 2014; Zuluaga et al., 2015). Such eclipses could be rare or have long periods and if periodicity is required for a search they would not be found (Quillen et al., 2014; Petrov et al., 2015). They could have an unusual light curve transit shape, and so would not be well fit by a planet transit or eclipsing binary light curve model (Meng et al., 2014; Dong et al., 2014; Rattenbury et al., 2015). The transits could be deeper than expected for a planet transit and so would be classified as a possible eclipsing binary and so ignored in planet transit searches.

During an occultation (Fig. 7.8), structure in an occulting disk can be measured on the scale of a stellar radius or ~ 0.01 AU (about one million km), a scale that is difficult or impossible to resolve directly. So if eclipsing exoplanetary ring systems are evident in light curves, they would allow detailed study of ring structure, potentially even giving constraints on their composition through time resolved spectroscopy or from their wavelength dependent reflection and transmission properties.

Ring system outer radii are larger than planetary radii. The probability of detecting an extended object in transit depends on the fractional solid angle of the object covered in its orbit about the host star.

A spherical object of diameter d object in orbit with semi-major axis a covers a band of area $2\pi da$ during one revolution, i.e. a solid angle of $2\pi d/a$ as seen from the star. An observer viewing the star with line of sight intersecting this band would see an eclipse of the star. The total solid angle covered by a sphere being 4π , the ratio $p = (2\pi d/a)/(4\pi) = d/(2a)$ gives the probability that an eclipse is seen from a distribution of systems during a survey that goes on long enough to include the period of the

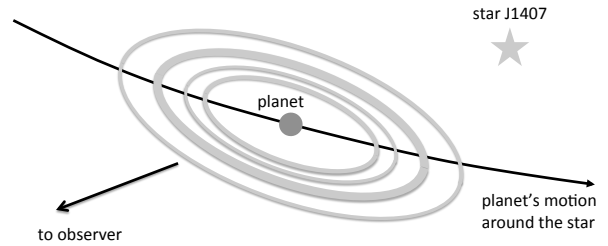


Figure 7.8 Sketch illustrating the modeling of possible rings around J1407b, the putative companion of J1407 (see text). During its motion around the star, an exoplanet surrounded by rings may cause the dimming of the star as seen by an observer (here far away on the lower left side of the figure). The sizes of the planet and its ring system are not on scale, they have been enlarged for better viewing.

orbit, taking into account all possible orientations and assuming a uniform distribution of orientations. If disks fill a large fraction of a secondary’s Hill radius, then the probability that a sample of young stars star exhibits eclipses could reach as high as 10^{-4} (see equation 14 of Mamajek et al. 2012).

With the discovery of the J1407 dimming event, it was argued from the number above that the probability of finding a dimming event by an eclipse of a circumsecondary or exoplanetary ring system in a large photometric survey is not small (Mamajek et al., 2012). A large uncertainty affecting the detection probability for eclipsing disks is the lifetime of circumplanetary and circumsecondary disks, with younger stars being most likely to host extended and dense circumplanetary or circumsecondary disks, and suggesting that young stellar populations would be most likely to exhibit disk or ring system eclipses.

The low fraction of field eclipsing binaries that exhibit disk like features suggests that the size and optical depth of ring systems and circumbinary disks decreases with age (Meng et al., 2014). A survey of 40,000 stars in the 2MASS calibration database that searched for dimming events and did not restrict the search to periodic light curves, primarily found new eclipsing binaries but also found dimming events from variable young stars (Quillen et al., 2014). The KELT photometric survey recently discovered long and deep dimming events from young stars. The 2014 dimming of RW Aurigae A was greater than 2 magnitudes and lasted 6 months (Petrov et al., 2015). The star RW Aur also exhibited a 6 month long 2 mag dip in 2010 (Rodriguez et al., 2013), while DM Ori exhibited, twice, dips of 1.5 mag lasting 6 months (Rodriguez et al., 2016). These types of events are sometimes called “dippers”. Even though the Kepler mission discovered thousands of short period planets in transit, none so far exhibit ring systems – perhaps short period planets cannot support extended ring systems (Hedman, 2015). Because they did not restrict their search to periodic systems or light curves that brighten, the citizen scientists in the Planet Hunters consortium recently discovered an F star, KIC 8462852, exhibiting irregularly shaped, aperiodic dips

Table 7.3. *Eclipsing Circumsecondary Disks*

Object	Eclipse length	Period	Depth ^a	Primary	Disk Temp.
EE Cep ^b	30-60 days	5.6 yr	0.6-2.1	B5eIII	900K
Epsilon Aurigae ^c	2 years	27.1 yr	0.8	F0 I	n.a.
OGLE-LMC-ECL-17782 ^d	2 days	13.35 days	0.5	B2	1200K
OGLE-LMC-ECL-11893 ^e	15 days	468 days	1.5	B9	6000K
OGLE-BLG 182.1.162852 ^f	100 days	3.5 years	1-2	n.a.	300 K
J1407 ^g	60 days	>4 years	4	K5V	200K

^aMeasured in magnitude drop. ^bGałań et al. (2012). ^cChadima et al. (2011). ^dMeng et al. (2014). ^eDong et al. (2014).

^fRattenbury et al. (2015). ^gKenworthy et al. (2015).

in flux down to below the 20% level (Boyajian et al., 2016). Surprisingly this star does not exhibit the behavior of a young star. The dips in the light curve might be explained with a dust cloud created by a destructive impact between two large planetesimals or families of evaporating comets (Bodman and Quillen, 2016). Another star, the white dwarf WD1145+017 exhibits 3-12 minute deep (0.5 mag) transit events (or dips) that could be due to disintegrating comets (Gänsicke et al., 2016). Recently more than twenty young (~ 10 Myr old) late-K and M dwarf stars were observed in the Kepler Mission K2 Campaign Field 2 that host proto-planetary disks and exhibit quasi-periodic or aperiodic dimmers (Ansdell et al., 2016). Magnetospheric truncation and accretion models can explain why dusty material is lifted out of the midplane to obscure the star causing the light curve dips and why so many young low mass stars are dimmers (Bodman et al., 2016).

7.6.1 Notes on individual objects

Two bright stars, EE-Cep and Epsilon Aurigae, have long been known to exhibit deep eclipses. These are both long period systems hosting circumsecondary eclipsing disks with early type primary stars. Both disks have radial structure such as a central clearing and in EE-Cep this causes asymmetry in the light curve (e.g., Gałań et al. 2012). Re-examination of eclipsing binary light curves in archival data have revealed three more eclipsing disk systems, OGLE-LMC-ECL-11893 with a 468 day period (Dong et al., 2014) and OGLE-BLG 182.1.162852, a bulge object with a 3.5 year period (Rattenbury et al., 2015) and OGLE-LMC-ECL-17782, exhibiting 2 day eclipses in a 13 day period; this likely host a transient B-star blow-out disk (Meng et al., 2014). Each eclipse of OGLE-LMC-ECL-11893 is remarkably similar and multi-color photometry shows that dust in the disk causes reddening (Dong et al., 2014). The eclipse shape can be fit with either a thin dusty disk or a thick gas and dust disk (Scott et al., 2014). Existing multicolor photometric observations could in the future be used to study the dust properties. These known eclipsing disk systems are listed in Table 7.3. Disk temperatures are estimated from the orbital period and the luminosity of the primary and span a wide range suggesting that these systems may in future provide interesting settings to study disk composition through spectroscopy.

An interesting case is J1407 (1SWASP J140747.93-394542.6), a 16 million year old, pre-main sequence K5-type star of some 0.9 solar mass in the Sco-Cen OB association. It exhibited a complex 54 day deep eclipse in April 2007, with a maximum depth greater than 3 magnitudes (Mamajek et al., 2012; van Werkhoven et al., 2014). The long eclipse was discovered in a Super Wide Angle Search for Planets (SuperWASP) light curve but a few data points from the All Sky Automated Survey (ASAS) confirmed that the star dropped in brightness in 2007. Continued monitoring and high contrast imaging rule out a bright or stellar secondary object (Kenworthy et al., 2015). An optically thick ring passing in front of the star, causes a change in slope (flux variation per unit time) dependent on the angular rotation rate of the ring (also see limits on radius of occulting objects in the KIC 8462852 system by Boyajian et al. 2016).

More detailed modelings of the slopes have been conducted by Kenworthy and Mamajek (2015) and Kenworthy et al. (2015), see Fig. 7.8. Using slope changes in the light curve, each corresponding to a ring edge, the J1407 eclipsing system has been modeled as a complex set of more than 35 thin rings lying in an oblique plane. The large slopes at some epochs suggest that the secondary object hosting the ring system orbits at no more than a few AU from the primary star on an eccentric orbit, with a period estimated from a few to some 30 years. The ringed object would be a giant planet of some 15-25 Jovian masses, while the ring system would contain about one Earth mass and span a diameter of about 180 millions km (1.2 AU). This can be compared to Saturn's rings, which contain about 10^{-5} Earth mass and is more than 600 times smaller than the system considered here.

The complex substructure suggests that the ring system is very thin and hosts moons that maintain sharp edges at Lindblad resonances, or open gaps in the disk. Crude estimations based on the width of one of these gaps suggest that it could stem from a Mars-size or small-Earth type object (Kenworthy and Mamajek, 2015). As more constraints of the disk thickness and planet mass are gathered, Eqs. 7.10 and 7.11 may be used to better assess the masses of those putative moons.

As a word of caution, we note that continued photometric monitoring of J1407 (Erin Scott, private communication) has not revealed new eclipse episodes, as is expected if the ringed planet has an orbital period of a few years. If ongoing

monitoring fails to find new eclipses over the next decades, then it may become impossible to account for the eclipse with an extended ring system orbiting a secondary object.

This said, an intriguing issue is the fact that the J1407 putative ring system would extend much beyond the planet Roche limit (usually some 2-3 planetary radii). These rings would then represent transient features en route towards an accretion process that will form a retinue of moons around the planet. Scaling from models of the proto-Jovian nebula, Mamajek et al. (2012) estimate that the lifetime of a circum-Jovian disk could be as long as several millions years, thus comparable to the age of J1407. However, this challenges the mainstream idea that rings exist only inside the Roche limit of their central planets, as accretion should proceed very rapidly (over a few orbital revolutions) to form moons. To prevent such outcome, Toomre’s parameter Q should be maintained just above unity. In that context, Eq. 7.4 can be re-written (Sicardy, 2006):

$$\frac{h}{a} \sim \frac{M_r}{M_p}, \quad (7.14)$$

assuming a uniform ring of radius a , mass M_r and thickness h surrounding a planet of mass M_p . For M_r comparable to Earth’s mass, M_p of some 20 Jovian masses and a a little bit above 1 AU (see above), this implies $h \sim 30,000$ km. At this point, the mechanism causing the stirring of the disk and maintaining this thickness remains to be explained.

7.7 Concluding remarks

As shown in this chapter, rings beyond the giant planets appear to be more common features than previously thought. This has important implications at different levels.

First, this raises the question of whether rings share some basic, universal physics, or, on the contrary, if they follow a wide variety of disconnected behaviors depending on the context. For instance, Chariklo’s rings and the material surrounding J1407b exhibit sharp edges or gaps, that are also encountered in Saturn’s and Uranus’ rings. Are those features all caused by shepherding nearby bodies (satellites or planets), or do they stem from other, yet to be described physical processes? In fact, none of the “moonlets” that are thought to be responsible for the narrow rings or gaps in the Saturnian C ring and Cassini Division have been discovered so far (Colwell et al., 2009). As high resolution imaging is steadily improving thanks to larger telescopes, adaptive optics or space instruments, it is now of paramount importance to discover (or rule out) the presence of confining bodies associated with sharp edges and gaps in the newly discovered rings.

At another level, rings can tell us a lot about the body they encircle. With the advent of the European Space Agency GAIA mission, star catalogs with absolute accuracy of a fraction of milliarcsec will be released soon. In that context, stellar occultations by Chariklo’s rings will be routinely observed by many teams. Those campaigns will then provide accuracies of better than one kilometer on the rings’

orbital elements. This might lead to the discovery of ring proper modes, as observed in Uranus’ rings (see the Chapter 4 by Nicholson *et al.*) and then provide the ring particles’ mean motion, a direct way to determine Chariklo’s mass, and thus its density through its dimensions. In the same vein, the rings’ precession rates could yield Chariklo’s dynamical oblateness J_2 , an important parameter to understand its internal structure. In short, rings may be precious probes of the gravity field of their host body.

Those programs are not restricted to Chariklo, but also aimed at searching for material around other Centaurs, TNOs and asteroids. This may lead to the discovery of new ring systems, or rule them out with a safe margin. It will then be possible to address on firmer ground the question of whether “small body” rings exist only around Centaurs, and why it is so, or if on the contrary, they are also present around very remote TNOs or even nearby asteroids. If exclusive to Centaurs, rings could be the witnesses of the troubled history of those objects (e.g. stemming from close encounters with giant planets), or a mere endogenous product associated with cometary activities of those bodies, or the outcome of a fine tuning of icy composition, size and temperature conditions, or the result of some other unknown processes.

As discussed in this chapter, rings might also have existed around the Saturnian satellite Iapetus and Rhea. However, those rings should have been quite different from each other, with a massive (relative to the satellite) disk that fell along Iapetus’ equator early in the history of the Solar System, and a relatively recent low-mass ring that sprinkled Rhea’s equator. In any case, they would be remnants of interesting processes, and would tell us how a collisional disk or an object can be driven toward a body through tidal interactions and fall onto its equator. In that vein, it is important to check – using well-sampled stellar occultations – if a ridge exists along Chariklo’s equator (or around other Centaurs). This would be a nice confirmation that rings may indeed explain Iapetus’ equatorial feature.

Turning to exoplanetary rings, we note that in 2012 transient events were considered uninteresting and completely ignored. The discovery of new eclipsing circumsecondary disks (Dong et al., 2014; Rattenbury et al., 2015), a candidate exoplanetary ring system (Mamajek et al., 2012; Kenworthy and Mamajek, 2015) and deep transient dimming events in both young and old stars from Kepler Mission data (Boyajian et al., 2016; Ansdell et al., 2016) imply that photometric observations can uncover new eclipsing disk systems.

Up to now all eclipsing and transient dimming events have been found in archival data, making it difficult to follow up non-periodic or long period eclipsing systems. In two cases, the same dimming events were found in more than one photometric archive, giving confirmation (J1407, Mamajek et al. 2012 and the dimming of V409 Tau, Rodriguez et al. 2013). Some of the dimming events seen in KIC 8462852 could have been detected from the ground. This system is now being monitored for new dimming events which may allow a multicolor photometric study. It is possible to mount a transient detection program that triggers on dimming events allowing multicolor or high cadence observations (and possibly spec-

troscopic observations) of rare, and long period, dimming events.

Future and more accurate photometric studies of larger populations of stars could detect dimmings caused by an exoplanetary ring system as rich and old as Saturn’s as well as counterparts at earlier epochs.

In that context, an interesting issue is the location of those rings relative to the exoplanet’s Roche limit. While Chariklo’s rings seem to lie a little bit outside of, but still near Chariklo’s Roche limit, the putative exoplanetary rings associated with J1407b are well outside that range. This undermines the paradigm of rings as collisional disks residing inside the Roche limit of the central body in order to prevent rapid accretion into individual objects. So, we are either very lucky to observe today the J1407b ring system before it coalesces into satellites, or our understanding of accretion time scales needs revisions. In any case, an estimation of the probability to detect by mere chance a ring system among all the transit events now observed is very much wanted. This might put constraints on the efficiency of confining mechanisms and on accretion time scales, thus allowing us to better understand the various steps that led to the formation of planets and satellites, including in our own Solar System.

B.S. acknowledges funding from the French grant “Beyond Neptune II” (ANR-11-IS56-0002) and from the European Research Council under the European Community’s H2020 (2014-2020/ ERC Grant Agreement no. 669416 “LUCKY STAR”). K.J.W. acknowledges funding from the NASA Origins program, and NASA SSERVI program (Institute of the Science of Exploration Targets) through institute grant number NNA14AB03A.

REFERENCES

- Ansdell, M., Gaidos, E., Rappaport, S. A., Jacobs, T. L., LaCourse, D. M., Jek, K. J., Mann, A. W., Wyatt, M. C., Kennedy, G., Williams, J. P., and Boyajian, T. S. 2016. Young “Dipper” Stars in Upper Sco and Oph Observed by K2. *Astrophys. J.*, **816**(Jan.), 69.
- Araujo, R. A. N., Sfair, R., and Winter, O. C. 2016. The rings of Chariklo under close encounters with the giant planets. *ArXiv e-prints*, Apr.
- Assafin, M., Camargo, J. I. B., Vieira Martins, R., Andrei, A. H., Sicardy, B., Young, L., da Silva Neto, D. N., and Braga-Ribas, F. 2010. Precise predictions of stellar occultations by Pluto, Charon, Nix, and Hydra for 2008-2015. *Astron. Astrophys.*, **515**(June), A32.
- Assafin, M., Camargo, J. I. B., Vieira Martins, R., Braga-Ribas, F., Sicardy, B., Andrei, A. H., and da Silva Neto, D. N. 2012. Candidate stellar occultations by large trans-Neptunian objects up to 2015. *Astron. Astrophys.*, **541**(May), A142.
- Belskaya, I. N., Bagnulo, S., Barucci, M. A., Muinonen, K., Tozzi, G. P., Fornasier, S., and Kolokolova, L. 2010. Polarimetry of Centaurs (2060) Chiron, (5145) Pholus and (10199) Chariklo. *Icarus*, **210**(Nov.), 472–479.
- Bockelée-Morvan, D., Lellouch, E., Biver, N., Paubert, G., Bauer, J., Colom, P., and Lis, D. C. 2001. Search for CO gas in Pluto, Centaurs and Kuiper Belt objects at radio wavelengths. *Astron. Astrophys.*, **377**(Oct.), 343–353.
- Bodman, E. H. L., and Quillen, A. 2016. KIC 8462852: Transit of a Large Comet Family. *Astrophys. J. Letters*, **819**(Mar.), L34.
- Bodman, E. H. L., Quillen, A. C., Ansdell, M., Hippke, M., Boyajian, T. S., Mamajek, E. E., Blackman, E. G., Rizzuto, A., and Kastner, J. H. 2016. Dippers and Dusty Disks Edges: A Unified Model. *ArXiv e-prints*, May.
- Boissel, Y., Sicardy, B., Roques, F., Gaulme, P., Doressoundiram, A., Widemann, T., Ivanov, V. D., Marco, O., Mason, E., Ageorges, N., Mousis, O., Rousselot, P., Dhillon, V. S., Littlefair, S. P., Marsh, T. R., Assafin, M., Braga Ribas, F., da Silva Neto, D., Camargo, J. I. B., Andrei, A., Vieira Martins, R., Behrend, R., and Kretlow, M. 2014. An exploration of Pluto’s environment through stellar occultations. *Astron. Astrophys.*, **561**(Jan.), A144.
- Boyajian, T. S., LaCourse, D. M., Rappaport, S. A., Fabrycky, D., Fischer, D. A., Gandolfi, D., Kennedy, G. M., Korhonen, H., Liu, M. C., Moor, A., Olah, K., Vida, K., Wyatt, M. C., Best, W. M. J., Brewer, J., Ciesla, F., Csák, B., Deeg, H. J., Dupuy, T. J., Handler, G., Heng, K., Howell, S. B., Ishikawa, S. T., Kovács, J., Kozakis, T., Kriskovics, L., Lehtinen, J., Lintott, C., Lynn, S., Nespral, D., Nikbakhsh, S., Schawinski, K., Schmitt, J. R., Smith, A. M., Szabo, G., Szabo, R., Viuhio, J., Wang, J., Weiksnar, A., Bosch, M., Connors, J. L., Goodman, S., Green, G., Hoekstra, A. J., Jebson, T., Jek, K. J., Omohundro, M. R., Schwengeler, H. M., and Szezwczyk, A. 2016. Planet Hunters IX. KIC 8462852 - where’s the flux? *Mon. Not. R. Astron. Soc.*, **457**(Apr.), 3988–4004.
- Braga-Ribas, F., Sicardy, B., Ortiz, J. L., Lellouch, E., Tancredi, G., Lecacheux, J., Vieira-Martins, R., Camargo, J. I. B., Assafin, M., Behrend, R., Vachier, F., Colas, F., Morales, N., Maury, A., Emilio, M., Amorim, A., Unda-Sanzana, E., Roland, S., Bruzzone, S., Almeida, L. A., Rodrigues, C. V., Jacques, C., Gil-Hutton, R., Vanzi, L., Milone, A. C., Schoenell, W., Salvo, R., Almenares, L., Jehin, E., Manfroid, J., Sposetti, S., Tanga, P., Klotz, A., Frappa, E., Caccia, P., Colque, J. P., Neves, C., Alvarez, E. M., Gillon, M., Pimentel, E., Giacchini, B., Roques, F., Widemann, T., Magalhães, V. S., Thirouin, A., Duffard, R., Leiva, R., Toledo, I., Capeche, J., Beisker, W., Pollock, J., Cedeño Montaña, C. E., Ivarsen, K., Reichart, D., Haislip, J., and Lacluyze, A. 2013. The Size, Shape, Albedo, Density, and Atmospheric Limit of Transneptunian Object (50000) Quaoar from Multichord Stellar Occultations. *Astrophys. J.*, **773**(Aug.), 26.
- Braga-Ribas, F., Sicardy, B., Ortiz, J. L., Snodgrass, C., Roques, F., Vieira-Martins, R., Camargo, J. I. B., Assafin, M., Duffard, R., Jehin, E., Pollock, J., Leiva, R., Emilio, M., Machado, D. I., Colazo, C., Lellouch, E., Skottfelt, J., Gillon, M., Ligier, N., Maquet, L., Benedetti-Rossi, G., Gomes, A. R., Kervella, P., Monteiro, H., Sfair, R., El Moutamid, M., Tancredi, G., Spagnotto, J., Maury, A., Morales, N., Gil-Hutton, R., Roland, S., Ceretta, A., Gu, S.-H., Wang, X.-B., Harpsøe, K., Rabus, M., Manfroid, J., Opitom, C., Vanzi, L., Mehret, L., Lorenzini, L., Schneiter, E. M., Melia, R., Lecacheux, J., Colas, F., Vachier, F., Widemann, T., Almenares, L., Sandness, R. G., Char, F., Perez, V., Lemos, P., Martinez, N., Jørgensen, U. G., Dominik, M., Roig, F., Reichart, D. E., Lacluyze, A. P., Haislip, J. B., Ivarsen, K. M., Moore, J. P., Frank, N. R., and Lambas, D. G. 2014. A ring system detected around the Centaur (10199) Chariklo. *Nature*, **508**(Apr.), 72–75.
- Burns, J. A., Showalter, M. R., Hamilton, D. P., Nicholson, P. D., de Pater, I., Ockert-Bell, M. E., and Thomas, P. C. 1999. The Formation of Jupiter’s Faint Rings. *Science*, **284**(May), 1146.
- Bus, S. J., Buie, M. W., Schleicher, D. G., Hubbard, W. B., Marcialis, R. L., Hill, R., Wasserman, L. H., Spencer, J. R., Millis, R. L., Franz, O. G., Bosh, A. S., Dunham, E. W., Ford, C. H., Young, J. W., Elliott, J. L., Meserole, R., Olkin, C. B., McDonald, S. W., Foust, J. A., Sopata, L. M., and Bandyopadhyay, R. M. 1996. Stellar Occultation by 2060 Chiron. *Icarus*, **123**(Oct.), 478–490.
- Camargo, J. I. B., Vieira-Martins, R., Assafin, M., Braga-Ribas, F., Sicardy, B., Desmars, J., Andrei, A. H., Benedetti-Rossi, G., and Dias-Oliveira, A. 2014. Candidate stellar occulta-

- tions by Centaurs and trans-Neptunian objects up to 2014. *Astron. Astrophys.*, **561**(Jan.), A37.
- Castillo-Rogez, J. C., Matson, D. L., Sotin, C., Johnson, T. V., Lunine, J. I., and Thomas, P. C. 2007. Iapetus' geophysics: Rotation rate, shape, and equatorial ridge. *Icarus*, **190**(Sept.), 179–202.
- Chadima, P., Harmanec, P., Bennett, P. D., Kloppenborg, B., Stencel, R., Yang, S., Božić, H., Šlechta, M., Kotková, L., Wolf, M., Škoda, P., Votruba, V., Hopkins, J. L., Buil, C., and Sudar, D. 2011. Spectral and photometric analysis of the eclipsing binary ϵ Aurigae prior to and during the 2009-2011 eclipse. *Astron. Astrophys.*, **530**(June), A146.
- Chiang, E. I., and Goldreich, P. 2000. Apse Alignment of Narrow Eccentric Planetary Rings. *Astrophys. J.*, **540**(Sept.), 1084–1090.
- Colwell, J. E., Nicholson, P. D., Tiscareno, M. S., Murray, C. D., French, R. G., and Marouf, E. A. 2009. *The Structure of Saturn's Rings*. Page 375.
- Cuzzi, J., Clark, R., Filacchione, G., French, R., Johnson, R., Marouf, E., and Spilker, L. 2009. *Ring Particle Composition and Size Distribution*. Page 459.
- Delsemme, A. H. 1982. Chemical composition of cometary nuclei. Pages 85–130 of: Wilkening, L. L. (ed), *IAU Colloq. 61: Comet Discoveries, Statistics, and Observational Selection*.
- Denk, T., Matz, K.-D., Roatsch, T., Wolf, U., Wagner, R. J., Neukum, G., and Jaumann, R. 2000 (Mar.). Iapetus (1): Size, Topography, Surface Structures, Craters. Page 1596 of: *Lunar and Planetary Science Conference*. Lunar and Planetary Inst. Technical Report, vol. 31.
- Denk, T., Neukum, G., Roatsch, T., McEwen, A. S., Turtle, E. P., Thomas, P. C., Helfenstein, P., Wagner, R. J., Porco, C. C., Perry, J. E., Giese, B., Johnson, T. V., Veverka, J., and Cassini Iss Team. 2005a (Mar.). First Imaging Results from the Iapetus B/C Flyby of the Cassini Spacecraft. In: Mackwell, S., and Stansbery, E. (eds), *36th Annual Lunar and Planetary Science Conference*. Lunar and Planetary Science Conference, vol. 36.
- Denk, T., Neukum, G., Helfenstein, P., Thomas, P. C., Turtle, E. P., McEwen, A. S., Roatsch, T., Veverka, J., Johnson, T. V., Perry, J. E., Owen, W. M., Wagner, R. J., Porco, C. C., and Cassini Iss Team. 2005b (Mar.). The First Six Months of Iapetus Observations by the Cassini ISS Camera. In: Mackwell, S., and Stansbery, E. (eds), *36th Annual Lunar and Planetary Science Conference*. Lunar and Planetary Science Conference, vol. 36.
- Desmars, J. 2015. Detection of Yarkovsky acceleration in the context of precovery observations and the future Gaia catalogue. *Astron. Astrophys.*, **575**(Mar.), A53.
- Desmars, J., Camargo, J. I. B., Braga-Ribas, F., Vieira-Martins, R., Assafin, M., Vachier, F., Colas, F., Ortiz, J. L., Duffard, R., Morales, N., Sicardy, B., Gomes-Júnior, A. R., and Benedetti-Rossi, G. 2015. Orbit determination of trans-Neptunian objects and Centaurs for the prediction of stellar occultations. *Astron. Astrophys.*, **584**(Dec.), A96.
- Dombard, A. J., Cheng, A. F., McKinnon, W. B., and Kay, J. P. 2012. Delayed formation of the equatorial ridge on Iapetus from a subsatellite created in a giant impact. *Journal of Geophysical Research (Planets)*, **117**(Mar.), 3002.
- Dong, S., Katz, B., Prieto, J. L., Udalski, A., Kozłowski, S., Street, R. A., Bramich, D. M., Tsapras, Y., Hundertmark, M., Snodgrass, C., Horne, K., Dominik, M., and Figuera Jaimes, R. 2014. OGLE-LMC-ECL-11893: The Discovery of a Long-period Eclipsing Binary with a Circumstellar Disk. *Astrophys. J.*, **788**(June), 41.
- Duffard, R., Pinilla-Alonso, N., Ortiz, J. L., Alvarez-Candal, A., Sicardy, B., Santos-Sanz, P., Morales, N., Colazo, C., Fernández-Valenzuela, E., and Braga-Ribas, F. 2014a. Photometric and spectroscopic evidence for a dense ring system around Centaur Chariklo. *Astron. Astrophys.*, **568**(Aug.), A79.
- Duffard, R., Pinilla-Alonso, N., Santos-Sanz, P., Vilenius, E., Ortiz, J. L., Mueller, T., Fornasier, S., Lellouch, E., Mommert, M., Pal, A., Kiss, C., Mueller, M., Stansberry, J., Delsanti, A., Peixinho, N., and Trilling, D. 2014b. "TNOs are Cool": A survey of the trans-Neptunian region. XI. A Herschel-PACS view of 16 Centaurs. *Astron. Astrophys.*, **564**(Apr.), A92.
- Duxbury, T. C., and Ocampo, A. C. 1988. Mars: Satellite and ring search from Viking. *Icarus*, **76**(Oct.), 160–162.
- Elliot, J. L., French, R. G., Meech, K. J., and Elias, J. H. 1984. Structure of the Uranian rings. I - Square-well model and particle-size constraints. *Astron. J.*, **89**(Oct.), 1587–1603.
- Elliot, J. L., Olkin, C. B., Dunham, E. W., Ford, C. H., Gilmore, D. K., Kurtz, D., Lazzaro, D., Rank, D. M., Temi, P., Bandyopadhyay, R. M., Barroso, J., Barucci, A., Bosh, A. S., Buie, M. W., Bus, S. J., Dahn, C. C., Foryta, D. W., Hubbard, W. B., Lopes, D. F., Marcialis, R. L., McDonald, S. W., Millis, R. L., Reitsema, H., Schleicher, D. G., Sicardy, B., Stone, R. P. S., and Wasserman, L. H. 1995. Jet-like features near the nucleus of Chiron. *Nature*, **373**(Jan.), 46–49.
- Elliot, J. L., Person, M. J., Zuluaga, C. A., Bosh, A. S., Adams, E. R., Brothers, T. C., Gulbis, A. A. S., Levine, S. E., Lockhart, M., Zangari, A. M., Babcock, B. A., Dupré, K., Pasachoff, J. M., Souza, S. P., Rosing, W., Secrest, N., Bright, L., Dunham, E. W., Sheppard, S. S., Kakkala, M., Tilleman, T., Berger, B., Briggs, J. W., Jacobson, G., Valleli, P., Volz, B., Rappoport, S., Hart, R., Brucker, M., Michel, R., Mattingly, A., Zambrano-Marin, L., Meyer, A. W., Wolf, J., Ryan, E. V., Ryan, W. H., Morzinski, K., Grigsby, B., Brimacombe, J., Ragozzine, D., Montano, H. G., and Gilmore, A. 2010. Size and albedo of Kuiper belt object 55636 from a stellar occultation. *Nature*, **465**(June), 897–900.
- Fornasier, S., Lellouch, E., Müller, T., Santos-Sanz, P., Panuzzo, P., Kiss, C., Lim, T., Mommert, M., Bockelée-Morvan, D., Vilenius, E., Stansberry, J., Tozzi, G. P., Mottola, S., Delsanti, A., Crovisier, J., Duffard, R., Henry, F., Lacerda, P., Barucci, A., and Gicquel, A. 2013. TNOs are Cool: A survey of the trans-Neptunian region. VIII. Combined Herschel PACS and SPIRE observations of nine bright targets at 70–500 μm . *Astron. Astrophys.*, **555**(July), A15.
- Fornasier, S., Lazzaro, D., Alvarez-Candal, A., Snodgrass, C., Tozzi, G. P., Carvano, J. M., Jiménez-Teja, Y., Silva, J. S., and Bramich, D. M. 2014. The Centaur 10199 Chariklo: investigation into rotational period, absolute magnitude, and cometary activity. *Astron. Astrophys.*, **568**(Aug.), L11.
- French, R. G., Nicholson, P. D., Porco, C. C., and Marouf, E. A. 1991. *Dynamics and structure of the Uranian rings*. Pages 327–409.
- Gałań, C., Mikołajewski, M., Tomov, T., Graczyk, D., Apostolovska, G., Barzova, I., Bellas-Velidis, I., Bilkina, B., Blake, R. M., Bolton, C. T., Bondar, A., Brát, L., Brožek, T., Budzisz, B., Cikała, M., Csák, B., Dapergolas, A., Dimitrov, D., Dobierski, P., Drahus, M., Drózdź, M., Dvorak, S., Elder, L., Frąckowiak, S., Galazutdinov, G., Gazeas, K., Georgiev, L., Gere, B., Goździewski, K., Grinin, V. P., Gromadzki, M., Hajduk, M., Heras, T. A., Hopkins, J., Iliev, I., Janowski, J., Kocián, R., Kołaczowski, Z., Kolev, D., Kopacki, G., Krzesiński, J., Kučáková, H., Kuligowska, E., Kundera, T., Kurpińska-Winiarska, M., Kuźmicz, A., Liakos, A., Lister,

- T. A., Maciejewski, G., Majcher, A., Majewska, A., Marrese, P. M., Michalska, G., Migaszewski, C., Miller, I., Munari, U., Musaev, F., Myers, G., Narwid, A., N emeth, P., Niarchos, P., Niemczura, E., Og oza, W.,  ogmen, Y., Oksanen, A., Osiwała, J., Peneva, S., Pigulski, A., Popov, V., Pych, W., Pye, J., Ragan, E., Roukema, B. F., R ożański, P. T., Semkov, E., Siwak, M., Staels, B., Stateva, I., Stempels, H. C., Stęślicki, M., Świerczyński, E., Szymański, T., Tomov, N., Waniak, W., Więcek, M., Winiarski, M., Wychudzki, P., Zajczyk, A., Zoła, S., and Zwitter, T. 2012. International observational campaigns of the last two eclipses in EE Cephei: 2003 and 2008/9. *Astron. Astrophys.*, **544**(Aug.), A53.
- G ansicke, B. T., Aungwerojwit, A., Marsh, T. R., Dhillon, V. S., Sahman, D. I., Veras, D., Farihi, J., Chote, P., Ashley, R., Arjyotha, S., Rattanasoon, S., Littlefair, S. P., Pollacco, D., and Burleigh, M. R. 2016. High-speed Photometry of the Disintegrating Planetesimals at WD1145+017: Evidence for Rapid Dynamical Evolution. *Astrophys. J. Letters*, **818**(Feb.), L7.
- Giese, B., Denk, T., Neukum, G., Roatsch, T., Helfenstein, P., Thomas, P. C., Turtle, E. P., McEwen, A., and Porco, C. C. 2008. The topography of Iapetus' leading side. *Icarus*, **193**(Feb.), 359–371.
- Gladman, B., Marsden, B. G., and Vanlaerhoven, C. 2008. *Nomenclature in the Outer Solar System*. Pages 43–57.
- Goldreich, P., and Porco, C. C. 1987. Shepherding of the Uranian Rings. II. Dynamics. *Astron. J.*, **93**(Mar.), 730.
- Goldreich, P., and Tremaine, S. 1979a. Precession of the epsilon ring of Uranus. *Astron. J.*, **84**(Oct.), 1638–1641.
- Goldreich, P., and Tremaine, S. 1979b. Towards a theory for the Uranian rings. *Nature*, **277**(Jan.), 97–99.
- Goldreich, P., and Tremaine, S. 1982. The dynamics of planetary rings. *Ann. rev. Astron. Astrophys.*, **20**, 249–283.
- Guilbert, A., Barucci, M. A., Brunetto, R., Delsanti, A., Merlin, F., Alvarez-Candal, A., Fornasier, S., de Bergh, C., and Sarid, G. 2009. A portrait of Centaur 10199 Chariklo. *Astron. Astrophys.*, **501**(July), 777–784.
- Guilbert-Lepoutre, A. 2011. A Thermal Evolution Model of Centaur 10199 Chariklo. *Astron. J.*, **141**(Mar.), 103.
- Hamilton, D. P. 1996. The asymmetric time-variable rings of Mars. *Icarus*, **119**(Jan.), 153–172.
- Hedman, M. M. 2015. Why Are Dense Planetary Rings Only Found between 8 AU and 20 AU? *Astrophys. J. Letters*, **801**(Mar.), L33.
- Hedman, M. M., Nicholson, P. D., Cuzzi, J. N., Clark, R. N., Filacchione, G., Capaccioni, F., and Ciarniello, M. 2013. Connections between spectra and structure in Saturn's main rings based on Cassini VIMS data. *Icarus*, **223**(Mar.), 105–130.
- Horner, J., Evans, N. W., and Bailey, M. E. 2004. Simulations of the population of Centaurs - I. The bulk statistics. *Mon. Not. R. Astron. Soc.*, **354**(Nov.), 798–810.
- Hyodo, R., Charnoz, S., Genda, H., and Ohtsuki, K. 2016. Formation of Centaurs's Rings through Their Partial Tidal Disruption during Planetary Encounters. *Astrophys. J. Letters*, **828**(Sept.), L8.
- Ip, W.-H. 2006. On a ring origin of the equatorial ridge of Iapetus. *Geophys. Res. Letters*, **33**(Aug.), 16203.
- Ishimoto, H. 1996. Formation of Phobos/Deimos Dust Rings. *Icarus*, **122**(July), 153–165.
- Jones, G. H., Roussos, E., Krupp, N., Beckmann, U., Coates, A. J., Cray, F., Dandouras, I., Dikarev, V., Dougherty, M. K., Garnier, P., Hansen, C. J., Hendrix, A. R., Hospodarsky, G. B., Johnson, R. E., Kempf, S., Khurana, K. K., Krimigis, S. M., Kr uger, H., Kurth, W. S., Lagg, A., McAndrews, H. J., Mitchell, D. G., Paranicas, C., Postberg, F., Russell, C. T., Saur, J., Seif, M., Spahn, F., Srama, R., Strobel, D. F., Tokar, R., Wahlund, J.-E., Wilson, R. J., Woch, J., and Young, D. 2008. The Dust Halo of Saturn's Largest Icy Moon, Rhea. *Science*, **319**(Mar.), 1380.
- Juhasz, A., and Horanyi, M. 1995. Dust torus around Mars. *J. Geophys. Res.*, **100**(Feb.), 3277–3284.
- Karkoschka, E. 2001. Comprehensive Photometry of the Rings and 16 Satellites of Uranus with the Hubble Space Telescope. *Icarus*, **151**(May), 51–68.
- Kenworthy, M. A., and Mamajek, E. E. 2015. Modeling Giant Extrasolar Ring Systems in Eclipse and the Case of J1407b: Sculpting by Exomoons? *Astrophys. J.*, **800**(Feb.), 126.
- Kenworthy, M. A., Lacour, S., Kraus, A., Triaud, A. H. M. J., Mamajek, E. E., Scott, E. L., S egransan, D., Ireland, M., Hamsch, F.-J., Reichart, D. E., Haislip, J. B., LaCluyze, A. P., Moore, J. P., and Frank, N. R. 2015. Mass and period limits on the ringed companion transiting the young star J1407. *Mon. Not. R. Astron. Soc.*, **446**(Jan.), 411–427.
- Krivov, A. V., and Hamilton, D. P. 1997. Martian dust belts: Waiting for discovery. *Icarus*, **128**(Aug.), 335–353.
- Krivov, A. V., and Titov, V. B. 1995. On the Dust Torus around the Orbit of PHOBOS. *Journal of Astrophysics and Astronomy Supplement*, **16**(Dec.), 394.
- Levison, H. F., Walsh, K. J., Barr, A. C., and Dones, L. 2011. Ridge formation and de-spinning of Iapetus via an impact-generated satellite. *Icarus*, **214**(Aug.), 773–778.
- Luu, J. X., and Jewitt, D. C. 1990. Cometary activity in 2060 Chiron. *Astron. J.*, **100**(Sept.), 913–932.
- Mamajek, E. E., Quillen, A. C., Pecaut, M. J., Moolekamp, F., Scott, E. L., Kenworthy, M. A., Collier Cameron, A., and Parley, N. R. 2012. Planetary Construction Zones in Occultation: Discovery of an Extrasolar Ring System Transiting a Young Sun-like Star and Future Prospects for Detecting Eclipses by Circumsecondary and Circumplanetary Disks. *Astron. J.*, **143**(Mar.), 72.
- Meech, K., and Belton, M. 1989. (2060) Chiron. *IAU Circ.*, Feb., 4770.
- Meng, Z., Quillen, A. C., Bell, C. P. M., Mamajek, E. E., Scott, E. L., and Zhou, J.-L. 2014. A search for eclipsing binaries that host discs. *Mon. Not. R. Astron. Soc.*, **441**(July), 3733–3741.
- Mosqueira, I., and Estrada, P. R. 2002. Apse Alignment of the Uranian Rings. *Icarus*, **158**(Aug.), 545–556.
- Murray, C. D., and Dermott, S. F. 1999. *Solar system dynamics*.
-  oieroset, M., Brain, D. A., Simpson, E., Mitchell, D. L., Phan, T. D., Halekas, J. S., Lin, R. P., and Acuna, M. H. 2010. Search for Phobos and Deimos gas/dust tori using in situ observations from Mars Global Surveyor MAG/ER. *Icarus*, **206**(Mar.), 189–198.
- Ortiz, J. L., Sicardy, B., Braga-Ribas, F., Alvarez-Candal, A., Lelouch, E., Duffard, R., Pinilla-Alonso, N., Ivanov, V. D., Littlefair, S. P., Camargo, J. I. B., Assafin, M., Unda-Sanzana, E., Jehin, E., Morales, N., Tancredi, G., Gil-Hutton, R., de La Cueva, I., Colque, J. P., da Silva Neto, D. N., Manfroid, J., Thirouin, A., Guti errez, P. J., Lecacheux, J., Gillon, M., Maury, A., Colas, F., Licandro, J., Mueller, T., Jacques, C., Weaver, D., Milone, A., Salvo, R., Bruzzone, S., Organero, F., Behrend, R., Roland, S., Vieira-Martins, R., Widemann, T., Roques, F., Santos-Sanz, P., Hestroffer, D., Dhillon, V. S., Marsh, T. R., Harlingten, C., Campo Bagatin, A., Alonso, M. L., Ortiz, M., Colazo, C., Lima, H. J. F., Oliveira, A. S., Kerber, L. O., Smiljanic, R., Pimentel, E., Giacchini, B., Cacella, P., and Emilio, M. 2012. Albedo and atmo-

- spheric constraints of dwarf planet Makemake from a stellar occultation. *Nature*, **491**(Nov.), 566–569.
- Ortiz, J. L., Duffard, R., Pinilla-Alonso, N., Alvarez-Candal, A., Santos-Sanz, P., Morales, N., Fernández-Valenzuela, E., Licandro, J., Campo Bagatin, A., and Thirouin, A. 2015. Possible ring material around centaur (2060) Chiron. *Astron. Astrophys.*, **576**(Apr.), A18.
- Pan, M., and Wu, Y. 2016. On the Mass and Origin of Chariklo’s Rings. *Astrophys. J.*, **821**(Apr.), 18.
- Peale, S. J. 1977. Rotation histories of the natural satellites. Pages 87–111 of: Burns, J. A. (ed), *IAU Colloq. 28: Planetary Satellites*.
- Petrov, P. P., Gahm, G. F., Djupvik, A. A., Babina, E. V., Artemenko, S. A., and Grankin, K. N. 2015. Another deep dimming of the classical T Tauri star RW Aurigae A. *Astron. Astrophys.*, **577**(May), A73.
- Pires dos Santos, P. M., Giuliatti Winter, S. M., Sfair, R., and Mourão, D. C. 2013. Small particles in Pluto’s environment: effects of the solar radiation pressure. *Mon. Not. R. Astron. Soc.*, **430**(Apr.), 2761–2767.
- Poppe, A., and Horányi, M. 2011. The effect of Nix and Hydra on the putative Pluto-Charon dust cloud. *Planet. Space Sci.*, **59**(Oct.), 1647–1653.
- Porco, C. C., Baker, E., Barbara, J., Beurle, K., Brahic, A., Burns, J. A., Charnoz, S., Cooper, N., Dawson, D. D., Del Genio, A. D., Denk, T., Dones, L., Dyudina, U., Evans, M. W., Giese, B., Grazier, K., Helfenstein, P., Ingersoll, A. P., Jacobson, R. A., Johnson, T. V., McEwen, A., Murray, C. D., Neukum, G., Owen, W. M., Perry, J., Roatsch, T., Spitale, J., Squyres, S., Thomas, P. C., Tiscareno, M., Turtle, E., Vasavada, A. R., Veverka, J., Wagner, R., and West, R. 2005. Cassini Imaging Science: Initial Results on Phoebe and Iapetus. *Science*, **307**(Feb.), 1237–1242.
- Porco, C. C., Thomas, P. C., Weiss, J. W., and Richardson, D. C. 2007. Saturn’s Small Inner Satellites: Clues to Their Origins. *Science*, **318**(Dec.), 1602–.
- Porter, S. B., and Stern, S. A. 2015. Orbits of Potential Pluto Satellites and Rings Between Charon and Hydra. *ArXiv e-prints*, May.
- Quillen, A. C., Ciocca, M., Carlin, J. L., Bell, C. P. M., and Meng, Z. 2014. Variability in the 2MASS calibration fields: a search for transient obscuration events. *Mon. Not. R. Astron. Soc.*, **441**(July), 2691–2716.
- Rattenbury, N. J., Wyrzykowski, L., Kostrzewa-Rutkowska, Z., Udalski, A., Kozłowski, S., Szymański, M. K., Pietrzyński, G., Soszyński, I., Poleski, R., Ulaczyk, K., Skowron, J., Pietrukowicz, P., Mróz, P., and Skowron, D. 2015. OGLE-BLG182.1.162852: an eclipsing binary with a circumstellar disc. *Mon. Not. R. Astron. Soc.*, **447**(Feb.), L31–L34.
- Robuchon, G., Choblet, G., Tobie, G., Čadež, O., Sotin, C., and Grasset, O. 2010. Coupling of thermal evolution and despinning of early Iapetus. *Icarus*, **207**(June), 959–971.
- Rodriguez, J. E., Pepper, J., Stassun, K. G., Siverd, R. J., Cargile, P., Beatty, T. G., and Gaudi, B. S. 2013. Occultation of the T Tauri Star RW Aurigae A by its Tidally Disrupted Disk. *Astron. J.*, **146**(Nov.), 112.
- Rodriguez, J. E., Stassun, K. G., Cargile, P., Shappee, B. J., Siverd, R. J., Pepper, J., Lund, M. B., Kochanek, C. S., James, D., Kuhn, R. B., Beatty, T. G., Gaudi, B. S., Weintraub, D. A., Stanek, K. Z., Holoiien, T. W. S., Prieto, J. L., Feldman, D. M., and Espillat, C. C. 2016. DM Ori: A Young Star Occulted by a Disturbance in its Protoplanetary Disk. *ArXiv e-prints*, July.
- Rousselot, P. 2008. 174P/Echeclus: a strange case of outburst. *Astron. Astrophys.*, **480**(Mar.), 543–550.
- Ruprecht, J. D., Bosh, A. S., Person, M. J., Bianco, F. B., Ful-ton, B. J., Gulbis, A. A. S., Bus, S. J., and Zangari, A. M. 2015. 29 November 2011 stellar occultation by 2060 Chiron: Symmetric jet-like features. *Icarus*, **252**(May), 271–276.
- Schenk, P., Hamilton, D. P., Johnson, R. E., McKinnon, W. B., Paranicas, C., Schmidt, J., and Showalter, M. R. 2011. Plasma, plumes and rings: Saturn system dynamics as recorded in global color patterns on its midsize icy satellites. *Icarus*, **211**(Jan.), 740–757.
- Scott, E. L., Mamajek, E. E., Pecaut, M. J., Quillen, A. C., Moolekamp, F., and Bell, C. P. M. 2014. Modeling Transiting Circumstellar Disks: Characterizing the Newly Discovered Eclipsing Disk System OGLE LMC-ECL-11893. *Astrophys. J.*, **797**(Dec.), 6.
- Scotti, J. V. 1997. Discovery of 1997 CU26. *Minor Planet Electronic Circulars*, Feb., D11.
- Showalter, M. R., and Hamilton, D. P. 2010. Potential for rings at Pluto. In: *Nix and Hydra: Five Years after Discovery Meeting*, Space Telescope Science Institute.
- Showalter, M. R., and Hamilton, D. P. 2015. Resonant interactions and chaotic rotation of Pluto’s small moons. *Nature*, **522**(June), 45–49.
- Showalter, M. R., Hamilton, D. P., and Nicholson, P. D. 2006. A deep search for Martian dust rings and inner moons using the Hubble Space Telescope. *Planet. Space Sci.*, **54**(Aug.), 844–854.
- Showalter, M. R., Hamilton, D. P., Stern, S. A., Weaver, H. A., Steffl, A. J., and Young, L. A. 2011. New Satellite of (134340) Pluto: S/2011 (134340) 1. *Central Bureau Electronic Telegrams*, **2769**(July), 1.
- Showalter, M. R., Weaver, H. A., Stern, S. A., Steffl, A. J., Buie, M. W., Merline, W. J., Mutchler, M. J., Soummer, R., and Throop, H. B. 2012. New Satellite of (134340) Pluto: S/2012 (134340) 1. *IAU Circular*, **9253**(July).
- Sicardy, B. 2006. Dynamics of Planetary Rings. Page 183 of: Souchay, J. (ed), *Dynamics of Extended Celestial Bodies and Rings*. Lecture Notes in Physics, Berlin Springer Verlag, vol. 682.
- Sicardy, B., Ortiz, J. L., Assafin, M., Jehin, E., Maury, A., Lelouch, E., Hutton, R. G., Braga-Ribas, F., Colas, F., Hestroffer, D., Lecacheux, J., Roques, F., Santos-Sanz, P., Widemann, T., Morales, N., Duffard, R., Thirouin, A., Castro-Tirado, A. J., Jelínek, M., Kubánek, P., Sota, A., Sánchez-Ramírez, R., Andrei, A. H., Camargo, J. I. B., da Silva Neto, D. N., Gomes, A. R., Martins, R. V., Gillon, M., Manfroid, J., Tozzi, G. P., Harlinton, C., Saravia, S., Behrend, R., Mottola, S., Melendo, E. G., Peris, V., Fabregat, J., Madieto, J. M., Cuesta, L., Eibe, M. T., Ullán, A., Organero, F., Pastor, S., de Los Reyes, J. A., Pedraz, S., Castro, A., de La Cueva, I., Muler, G., Steele, I. A., Cebrián, M., Montañés-Rodríguez, P., Oscoz, A., Weaver, D., Jacques, C., Corradi, W. J. B., Santos, F. P., Reis, W., Milone, A., Emilio, M., Gutiérrez, L., Vázquez, R., and Hernández-Toledo, H. 2011. A Pluto-like radius and a high albedo for the dwarf planet Eris from an occultation. *Nature*, **478**(Oct.), 493–496.
- Sicardy, B., Braga-Ribas, F., Ortiz, J. L., Vieira-Martins, R., Colas, F., Duffard, R., Camargo, J. I., Desmars, J., Gulbis, A., Assafin, M., Maquet, L., Beisker, W., Benedetti-Rossi, G., Vachier, F., Dumas, C., Ivanov, V. D., Renner, S., Bath, K.-L., Klotz, A., Pollock, J. T., Lecacheux, J., Dauvergne, J.-L., Peyrot, A., and Teng, J.-P. 2014 (Nov.). Dense and narrow rings around the Centaur object (10199) Chariklo.

- Page 408.01 of: *AAS/Division for Planetary Sciences Meeting Abstracts*. AAS/Division for Planetary Sciences Meeting Abstracts, vol. 46.
- Singer, K. N., McKinnon, W. B., and Schenk, P. M. 2013 (Mar.). Large Landslides on Icy Satellites: New Examples from Rhea and Tethys. Page 2955 of: *Lunar and Planetary Science Conference*. Lunar and Planetary Science Conference, vol. 44.
- Smith, B. A., Soderblom, L., Beebe, R. F., Boyce, J. M., Briggs, G., Bunker, A., Collins, S. A., Hansen, C., Johnson, T. V., Mitchell, J. L., Terrile, R. J., Carr, M. H., Cook, A. F., Cuzzi, J. N., Pollack, J. B., Danielson, G. E., Ingersoll, A. P., Davies, M. E., Hunt, G. E., Masursky, H., Shoemaker, E. M., Morrison, D., Owen, T., Sagan, C., Veverka, J., Strom, R., and Suomi, V. E. 1981. Encounter with Saturn - Voyager 1 imaging science results. *Science*, **212**(Apr.), 163–191.
- Smith, B. A., Soderblom, L., Batson, R. M., Bridges, P. M., Inge, J. L., Masursky, H., Shoemaker, E., Beebe, R. F., Boyce, J., Briggs, G., Bunker, A., Collins, S. A., Hansen, C., Johnson, T. V., Mitchell, J. L., Terrile, R. J., Cook, A. F., Cuzzi, J. N., Pollack, J. B., Danielson, G. E., Ingersoll, A. P., Davies, M. E., Hunt, G. E., Morrison, D., Owen, T., Sagan, C., Veverka, J., Strom, R., and Suomi, V. E. 1982. A new look at the Saturn system - The Voyager 2 images. *Science*, **215**(Jan.), 504–537.
- Soter, S. 1971. *The dust belts of Mars*. Cornell CRSR Report #462.
- Spencer, J. R., Showalter, M. R., Stern, S. A., Brozovic, M., Buie, M. W., Hamilton, D. P., Jacobson, R. A., Kaufmann, D. E., Lauer, T. R., Parker, A. H., Porter, S. B., Throop, H. B., Verbiscer, A. J., Weaver, H. A., Young, L. A., Ennico, K., and Olkin, C. B. 2015 (Nov.). Small Satellites and Dust in the Pluto System: Upper Limits and Implications. Page 101.05 of: *AAS/Division for Planetary Sciences Meeting Abstracts*. AAS/Division for Planetary Sciences Meeting Abstracts, vol. 47.
- Steffl, A. J., and Stern, S. A. 2007. First constraints on rings in the Pluto system. *Astron. J.*, **133**(Apr.), 1485–1489.
- Stern, S. A., Weaver, H. A., Steffl, A. J., Mutchler, M. J., Merline, W. J., Buie, M. W., Young, E. F., Young, L. A., and Spencer, J. R. 2006. A giant impact origin for Pluto’s small moons and satellite multiplicity in the Kuiper belt. *Nature*, **439**(Feb.), 946–948.
- Tenishev, V., Combi, M. R., and Rubin, M. 2011. Numerical Simulation of Dust in a Cometary Coma: Application to Comet 67P/Churyumov-Gerasimenko. *Astrophys. J.*, **732**(May), 104.
- Thomas, P. C. 2010. Sizes, shapes, and derived properties of the saturnian satellites after the Cassini nominal mission. *Icarus*, **208**(July), 395–401.
- Thomas, P. C., Burns, J. A., Helfenstein, P., Squyres, S., Veverka, J., Porco, C., Turtle, E. P., McEwen, A., Denk, T., Giese, B., Roatsch, T., Johnson, T. V., and Jacobson, R. A. 2007. Shapes of the saturnian icy satellites and their significance. *Icarus*, **190**(Oct.), 573–584.
- Throop, H. B., French, R. G., Shoemaker, K., Olkin, C. B., Ruhland, T. R., and Young, L. A. 2015. Limits on Pluto’s ring system from the June 12 2006 stellar occultation and implications for the New Horizons impact hazard. *Icarus*, **246**(Jan.), 345–351.
- Tiscareno, M. S. 2013. *Planetary Rings*. Page 309.
- Tiscareno, M. S., Burns, J. A., Cuzzi, J. N., and Hedman, M. M. 2010. Cassini imaging search rules out rings around Rhea. *Geophys. Res. Letters*, **37**(July), L14205.
- Tiscareno, M. S., Hedman, M. M., Burns, J. A., and Castillo-Rogez, J. 2013. Compositions and Origins of Outer Planet Systems: Insights from the Roche Critical Density. *Astrophys. J. Letters*, **765**(Mar.), L28.
- van Werkhoven, T. I. M., Kenworthy, M. A., and Mamajek, E. E. 2014. Analysis of 1SWASP J140747.93-394542.6 eclipse fine-structure: hints of exomoons. *Mon. Not. R. Astron. Soc.*, **441**(July), 2845–2854.
- Weaver, H. A., Stern, S. A., Mutchler, M. J., Steffl, A. J., Buie, M. W., Merline, W. J., Spencer, J. R., Young, E. F., and Young, L. A. 2006. Discovery of two new satellites of Pluto. *Nature*, **439**(Feb.), 943–945.
- Zuluaga, J. I., Kipping, D. M., Sucerquia, M., and Alvarado, J. A. 2015. A Novel Method for Identifying Exoplanetary Rings. *Astrophys. J., Letters*, **803**(Apr.), L14.